Revision 2: correction data August 9, 2013

Scheelite Elemental and Isotopic Signatures: Implications for the Genesis of Skarn-Type W-Mo Deposits in the Chizhou Area, Eastern China

GUOXUE SONG[1], KEZHANG QIN[1], GUANGMING LI[1], NOREEN J. EVANS[2] and LEI CHEN[3]

[1]Key Laboratory of Mineral Resources, Institute of Geology and Geophysics, Chinese Academy of Sciences, Beijing 100029, China
[2]John de Laeter Centre for Isotope Research, Applied Geology, Curtin University, Perth, Australia
[3]Institute of Mineral Resources Chinese Academy of Geological Sciences, Beijing 100037, China

ABSTRACT

Scheelite is well developed in hydrothermal deposits, providing a window into genetic processes and facilitating comparative studies, however few studies have focused on characterizing scheelite in skarn-type W-Mo deposits. The primary ore mineral in the Jitoushan and Baizhangyan skarn-type W-Mo deposits (Eastern China), scheelite was analysed for major, trace and rare earth element (REE) abundance and for Sr-Nd isotopes. The analysis revealed two unique geochemical characteristics that distinguish the scheelite from skarn-type W-Mo to that from vein-type Au-W and porphyry-type W-Mo deposits: higher Mo content with a negative correlation between MoO_3 and WO_3 and a strong HREE depletion.

Skarn-type W-Mo scheelite mainly inherited REE signatures from ore-forming fluids and the early precipitation of skarn minerals (e.g., garnet, diopside and amphibole) has most likely resulted in the observed strong HREE depletion in scheelite and the decoupling of LREEs and HREEs. Of the numerous substitution mechanisms suggested by previous workers, $3Ca^{2+}=2REE^{3+}+\square Ca$ (where $\square Ca$ is a Ca site vacancy) is preferred for the substitution of REE^{3+} for Ca^{2+} and in this study, particularly given the low salinity of ore fluids.

As the scheelite Eu anomalies were inherited from ore-forming fluids with variable redox conditions and pH, the complex δEu/Mo correlation indicates that Mo increasingly entered the scheelite under oxidizing conditions and reached a maxim at δEu values of 0.8 to 1. In contrast, under reducing conditions, Mo contents in scheelite decrease gradually and Mo is precipitated as molybdenite as a result of the change in dominant valence state.

Unlike the Sr-Nd isotope compositions of scheelite from vein-type Au-(W) and

W-(Sb-Au) deposits, the scheelite from skarn-type W-Mo deposits has low ($^{143}Nd/^{144}Nd$)(t) (most < 0.5125) and intermediate ($^{87}Sr/^{86}Sr$)(t) values (most between 0.708 and 0.715). The εNd(t) values of the scheelite varied from -16 to -12.3 in the Baizhangyan deposit and from -9.5 to -9.1 in the Jitoushan deposit, indicating that the ore-forming materials in the two W-Mo deposits were mainly derived from crustal sources.

Key words: skarn-type, scheelite, trace element, substitution, REE, Sr-Nd isotope, Eu anomaly, W-Mo deposits, Chizhou.

INTRODUCTION

Scheelite ($CaWO_4$) is well developed in skarn- and porphyry-type deposits, and is also developed in quartz vein- and a few metamorphic-type deposits (Allen and Folinsbee 1944; Xu 1957; Noble et al. 1984; Liu 1987; Zhang et al. 1990; Uspensky et al. 1998; Peng et al. 2003; Wang et al. 2008). It is a hydrothermal mineral whose precipitation is often spatially and temporally related to that of gold, molybdenite, chalcopyrite and cassiterite. It is of particular interest to ore geologists because it has the potential to provide important information on the genesis of ore minerals and their related deposits (Zhang et al. 1990; Brugger et al. 2008). For example, it can be used to resolve the long-standing problem of directly dating gold or tungsten deposits (Anglin et al. 1996; Brugger et al. 2002).

Due to their similar electron configurations and ionic radii, elements such as rare earth elements (REEs), Sr, Nd, Y and Pb could substitute for Ca^{2+} in the scheelite structure (Cottrant 1981; Raimbault et al. 1993). Hence, scheelite contains abundant trace elements and REEs and has high Sm/Nd ratios and low Rb/Sr ratios (Deer et al. 1966; Cottrant 1981; Bell et al. 1989; Voicu et al. 2000; Brugger et al. 2000, 2002, 2008). Because the REE composition of scheelite can provide information about magmatic melts and ore-forming fluids (Cottrant 1981), different REE patterns indicate different source materials and mineralization conditions (Tomschi 1986; Wang et al. 2010). Subtle changes in scheelite ΣREE+Y and REE curves indicate that the magma and fluids, which came from the same source, may have differentiated and evolved in different ways (Henderson 1985; Zhang et al. 1990; Raimbault et al. 1993; Sylvester and Ghaderi 1997; Zeng et al. 1998; Brugger et al. 2002, 2008; Dostal et al. 2009).

Because the scheelite lattice can accommodate limited Sr but rejects Rb (Deer et al. 1966) and the radiogenic ^{87}Sr from ^{87}Rb has a modest effect on Sr isotope composition, the scheelite Rb-Sr isotopic system could be used to trace the source of ore-forming fluids (Bell et al. 1989). In comparison, both Sm^{3+} and Nd^{3+} can enter the scheelite lattice by replacing Ca^{2+}, and Nd has a similar solubility to Sm in the form of

NdF_3 or $NdCl_3$ in hydrothermal fluids (Migdisov et al. 2006, 2009). Scheelite Sm/Nd ratios are relatively stable in fluid systems with stable physicochemical conditions and, therefore, the Sm-Nd isotope system can be used to both date the mineralization and trace the sources of ore-forming fluids (Bell et al. 1989; Anglin et al. 1996; Ghaderi et al. 1998; Zhao and Jiang 2004; Roberts et al. 2006; Liu et al. 2007; Peng et al. 2008; Zhang et al. 2008).

Most studies have focused on scheelite from vein-type W, Au-(W) or W-Sb-Au deposits, with few focusing on scheelite from skarn-type W-Mo deposits. This study examines the in situ major and trace element signatures, REE compositions and Sr-Nd isotope geochemistry of scheelite from the recently discovered skarn-type W-Mo deposits in the south of the middle-lower Yangtze Valley, and expounds on their genesis and significance. Synthesized with previous studies, scheelite REE patterns, Eu anomalies and Sr-Nd isotope compositions elucidate the evolution of ore-forming fluids and the ore genesis of these skarn-type W-Mo deposits.

GEOLOGY SETTING

The middle-lower Yangtze Valley is an important copper, iron and gold polymetallic metallogenic belt in Eastern China (Hu et al. 1977; Ishihara et al. 1986; Wang and Qin 1989; Chang et al. 1991; Zhai et al. 1992; Qin et al. 1999; Li 2001; Mao et al. 2003; Zhou et al. 2008; Song et al. 2012), and intensive studies have been conducted on the area. In recent years, many new W-Mo deposits such as Qimen (Qin et al. 2010), Gaojiabang (Jiang et al. 2009) and Guilinzheng have been discovered through continuous prospecting in the south of the Yangtze Valley metallogenic belt (YVMB). Some old W-Mo deposits, such as those in Matou, Baizhangyan and Jitoushan, have also increased reserves (Song et al. 2008, 2010). These discoveries have revealed a potential new source of Mo-W-Pb-Zn in the south of the YVMB (Song et al. 2012, 2013), located in the transition zone between the lower Yangtze depression and the Jiangnan ancient continent (JAC) (Fig. 1).

FIGURE 1. Regional geologic-tectonic sketch map of the middle-lower Yangtze Valley (revised from Mao et al. 2003; Song 2010).

As typical skarn-type W-Mo deposits in the Mo-W-Pb-Zn belt, Jitoushan and Baizhangyan have similar geological characteristics (Song et al. 2012, 2013). Both of the deposits are located on the rim of the Qingyang-Jiuhua complex, and the ore bodies occur in the contact zone between the Sinian-Cambrian limestone strata and the acid intrusive mass (Fig. 2a). Skarn-type W-Mo ore bodies are the main ore type with corresponding mineralizing porphyry masses detected at depth. (Fig. 2b, 2c). The W ore bodies are located above and outside the Mo ore bodies both vertically and horizontally. The Mo ore bodies mainly occur inside the porphyry mass and the skarn deposits close to the mass, whereas the W ore bodies mainly occur inside the skarn away from the porphyry mass. The main ore minerals are scheelite and molybdenite,

and the gangue minerals are garnet, diopside, epidote, quartz and calcite (Figs. 3a-1, 3a-2, 3b-1, 3b-2; Fig. 4). The scheelite was precipitated at the oxide stage following the skarn stage (Fig. 4). The typical alteration zones developed from the mass towards the wallrock via potassic alteration, silicate alteration, quartz sericitization, skarnization and finally carbonation. The W-Mo ore bodies mainly occur in the silication, quartz sericitization and skarnization zones. The Jitoushan and Baizhangyan W-Mo deposits were both formed during the Early Cretaceous epoch (Song et al. 2012, 2013).

FIGURE 2. (a) Regional geological sketch map of the Chizhou area. Geological map of the (b) Jitoushan and (c) Baizhangyan W-Mo deposits in the Chizhou area of the MLYV (adapted from Song et al. 2008).

FIGURE 3. Hand specimen photographs, microphotographs and cathode luminescence images of partial W-Mo ores from the Jitoushan and Baizhangyan W-Mo deposits. (a)-(e): W-Mo ores from the Jitoushan deposit; (f)-(h): W-Mo ores from the Baizhangyan deposit; (a) and (f): hand specimen photographs; (a') and (f') hand specimen photographs under ultraviolet light; (b), (c), (g) and (h): microphotographs; (d), (e), (i) and (j): cathode luminescence images. Grt=garnet, Ep=epidote, Qtz=quartz, Sch=scheelite, Cc=calcite.

FIGURE 4. The growth sequence of the main minerals in the Jitoushan and Baizhangyan skarn deposits.

SAMPLES AND ANALYTICAL METHODS

Scheelite samples

Scheelite samples P580-5, Jts-27-2 and P510-4 from the Jitoushan W-Mo deposit were taken from skarn ores containing garnet, diopside, scheelite, epidote, quartz, pyrite and molybdenite (Fig. 3). Scheelite samples B1-1, B5-6, B3-7 and B3-1 from the Baizhangyan W-Mo deposit were taken from skarn ores containing garnet, diopside, scheelite, epidote, hornblende, quartz, molybdenite and calcite (Fig. 3). The selected samples were prepared as polished probe sections for in situ electron probe and laser ablation inductively coupled plasma mass spectrometry (LA-ICP-MS) analysis. For the Sr-Nd isotope analysis, scheelite samples P580-5, Jts-27, Jt49 and P510-4 from the Jitoushan deposit and B3-1, B5-6-2 and B5-2 from the Baizhangyan deposit were selected from skarn W-Mo ores.

Electron probe analytical method

Major element compositions were obtained by wavelength-dispersive spectrometry using a JEOL JXA8100 electron probe operating at an accelerating voltage of 15 kV with a 12 nA beam current, 5 μm beam spot and 10-30 s counting time. The precision of all analyzed elements was better than 1.5%. Natural minerals and synthetic oxides were used as standards, and a program based on the ZAF procedure was used for data correction.

LA-ICP-MS analytical method

LA-ICP-MS analysis was performed at the State Key Laboratory of Geological Processes and Mineral Resources at the China University of Geosciences. Laser sampling was performed using an ArF excimer laser ablation system (193 nm wavelength), coupled to an Agilent 7500a ICP-MS with a 1 m transfer tube. Helium is advantageous as a carrier gas (Eggins et al. 1998; Günther and Heinrich, 1999) and was thus applied in this study. Argon was used as the make-up gas and mixed with the carrier gas via a T-connector before entering the ICP. The carrier and make-up gas flows were optimized by ablating the NIST SRM 610 to obtain maximum signal intensities while keeping low ThO/Th (0.1-0.3%) and Ca^{2+}/Ca^{+} (0.4-0.7%) ratios to reduce the oxide and doubly charged ion interferences. The $^{238}U/^{232}Th$ ratio, used as an indicator of complete vaporization, was kept at approximately 1 while ablating NIST SRM 610. A micro-flow PFA-100 self-aspirating Teflon nebulizer was used for solution ICP-MS analysis. The detailed operating conditions for the laser and ICP-MS instrument and the choice of isotopes are respectively listed in Tables 1 and 2. Each LA-ICP-MS analysis incorporated an approximately 30 s background acquisition (gas blank) followed by a 50 s data acquisition from the sample. Every eighth spot analysis was followed by one NIST SRM 610 analysis to correct the time-dependent drift of sensitivity and mass discrimination of the ICP-MS (Liu et al. 2008). Reference glasses (MPI-DING) were analyzed prior to and after the sample analyses measurements (MACS-3, GP-4 and natural calcite). All analyses were acquired using time-resolved software.

Sr-Nd isotope analytical method

About 30 mg (to a precision of 0.01 mg) of scheelite were spiked with ^{149}Sm-^{150}Nd. The sample was dissolved in a mixture of 2 mL of 22 M HF, 1 mL of 15 M HNO_3 and 0.2 mL of $HClO_4$ in steel-jacketed Teflon digestion vessels and heated in an oven at 190 ^{o}C for 5 days. After drying down on a hot plate at 150 ^{o}C, 4 mL of 6 M HCl were added and evaporated to dryness again. The sample residues were then leached using 1 mL of 2.5 M HCl, again in steel-jacketed Teflon digestion vessels, at 150 ^{o}C for 1 day. Finally, the sample solution was centrifuged at 4,000 RPM for 10 min.

The supernatant was loaded onto the pre-conditioned AG 50W*12 columns to separate Sr and REEs from the sample matrix. After rinsing four times with 0.5 mL of 2.5 M HCl, the column was washed with 8 mL of 5 M HCl to remove the matrix elements. After this step, the Sr was stripped with 2 mL of 5 M HCl, and the REEs were then stripped with 8 mL of 6 M HCl. The REE fraction obtained from the cation-exchange column was dried down and taken up with 0.2 mL of 0.07 M HCl and then loaded onto the pre-conditioned Eichrom-LN columns. After rinsing four times with 0.2 mL of 0.07 M HCl, the La, Ce and 80% of the Pr were eluted with 35 mL of 0.07 M HCl. The Nd was subsequently stripped with 12 mL of 0.14 M HCl, and the Sm was then stripped with 8 mL of 0.4 M HCl.

The Nd, Sm and Sr isotopes were analyzed on an IsoProbe-T thermal ionization mass spectrometer (TIMS) (Isotopx, formerly GV Instruments, England), installed at the Institute of Geology and Geophysics, Chinese Academy of Sciences (IGGCAS).

The Nd isotopes were determined as NdO^+ using a single tungsten filament with TaF_5 as an ionization activator (Chu et al. 2009, 2012). The measured $^{143}Nd/^{144}Nd$ ratios were corrected for mass fractionation using $^{146}Nd/^{144}Nd=0.7219$. During data collection, the measured value for the JNdi-1 Nd standard was $^{143}Nd/^{144}Nd=0.512117\pm10$ (2δD, n=8). The Sm isotopes were analyzed as Sm^+ using a single Ta filament.

Sr isotopes were also determined using a single tungsten filament with TaF_5 as an ionization activator, as described in detail by Li et al. (2005). The Sr isotope ratios were corrected for mass fractionation using $^{86}Sr/^{88}Sr=0.1194$. The measured value for the Sr standard NBS987 during the course of this study was $^{87}Sr/^{86}Sr=0.710245\pm18$ (2δD, n=8).

RESULTS

Major element compositions

A total of 14 major element analyses were conducted on scheelite samples from W-Mo deposits in Baizhangyan and Jitoushan. The representative analyses are reported in Table 1. The scheelite from Baizhangyan had WO_3 concentrations of 75.8-79.1%, CaO concentrations of 19.1-19.7%, MoO_3 concentrations of 1.08-5.2%, ZnO concentrations of <0.01-0.04%, FeO concentrations of <0.01-0.17% and MnO concentrations of 0.01-0.08%. The scheelite from Jiroushan had WO_3 concentrations of 77-81.7%, CaO concentrations of 19.1-19.6%, MoO_3 concentrations of 0.43-3.55%, CuO concentrations of 0-0.07%, PbO concentrations of <0.01-0.07%, ZnO concentrations of 0.01-0.21%, FeO concentrations of <0.01-0.45% and MnO concentrations of <0.01-0.05%. All of the scheelite samples had very low concentrations of CuO, ZnO, PbO, FeO and MnO and higher concentrations of MoO_3.

Trace element and rare earth element compositions

A total of 61 LA-ICP-MS trace element analyses were conducted on 8 scheelite samples from Baizhangyan and Jitoushan. The representative analyses are reported in Table 2 and the REE_N patterns for the analyses are presented in Figure 6. The scheelite from Baizhangyan had an Mo content of 20,000-180,000 ppm, a Cu content of <0.01-16 ppm, a Pb content of 2-35 ppm, a Zn content of <0.01-29 ppm, an Sn content of <0.01-0.4 ppm, an Sr content of 50-260 ppm and an Rb content of <0.01-0.2 ppm. The scheelite from Jitoushan had an Mo content of 7,000-60,000 ppm, a Cu content of <0.01-22 ppm, a Pb content of 1-6 ppm, a Zn content of <0.01-21 ppm, an Sn content of <0.01-1.3 ppm, an Sr content of 120-500 ppm and an Rb content of <0.01-0.4 ppm.

The scheelite samples from the two deposits yielded typical right-dip-type REE_N

patterns (Figs. 6, 1-8), enriched in light rare earth elements (LREEs) and depleted in heavy rare earth elements (HREEs) with a positive to negative Eu anomaly. The total REE (ΣREE+Y) of the scheelite samples ranged from 93.2-611 ppm, and the majority of results were above 100 ppm. The $LREE/HREE_N$ values ranged from 4.63-649 with most results between 50 and 300. The Eu/Eu^*_N (δEu) values ranged from 0.18-8.61 with the majority < 1 (scheelite δEu values for Jitoushan were all < 1). The $\Sigma REE+Y_N$, $LREE/HREE_N$ and Eu/Eu^*_N values of the scheelite samples from the Jitoushan deposit were generally lower than those from the Baizhangyan deposit. The scheelite samples were divided into two main types on the basis of their REE patterns: type I (S1), which had a positive Eu anomaly, and type II (S2), which had a negative Eu anomaly (Figs. 6, 1-8). The scheelite samples from the Baizhangyan deposit had both types of REE patterns (Figs. 6, 1-5), whereas the scheelite samples from the Jitoushan deposit had only the S2-type REE pattern (Figs. 6, 6-8).

Sr-Nd isotope compositions

The Sm-Nd and Sr isotope data for three scheelite samples from the Baizhangyan deposit and four samples from the Jitoushan W-Mo deposit are shown in Table 2. The results showed considerable variation in Sm (0.84-2.85 ppm), Nd (9.24-26.23 ppm) and Sr (87.8-533 ppm) concentrations (Table 3). The scheelite $^{147}Sm/^{144}Nd$ ratios ranged from 0.04513-0.13169 and the $^{143}Nd/^{144}Nd$ ratios ranged from 0.51176-0.51206. The $(^{143}Nd/^{144}Nd)(t)$, εNd(t) and $(^{87}Sr/^{86}Sr)(t)$ values for the scheelite from the 137 Ma Jitoushan deposit (Song et al. 2012) were 0.51164-0.51183, -16.0 to -12.3 and 0.70946-0.70974, respectively. The $(^{143}Nd/^{144}Nd)(t)$, εNd(t) and $(^{87}Sr/^{86}Sr)(t)$ values for the scheelite from the 134 Ma Baizhangyan deposit (Song et al. 2013) were 0.51198-0.51200, -9.5 to -9.1 and 0.71245-0.71738, respectively. The Sr-Nd isotopic compositions of the scheelite from Jitoushan were higher than those of the scheelite from Baizhangyan (Table 3).

Table 1. Results of scheelite major element analysis from the Baizhangyan and Jitoushan W-Mo deposits in the Chizhou area, Eastern China (%).

Table 2. Results of scheelite REE and trace element analysis from the Baizhangyan and Jitoushan W-Mo deposits in the Chizhou area, Eastern China (*ppm).

Table 3. Results of scheelite Sr-Nd isotopic analysis from the Baizhangyan and Jitoushan W-Mo deposits in the Chizhou area, Eastern China.

Table 4. Comparison of scheelite Sr-Nd isotopic analyses from hydrothermal deposits around the world.

DISCUSSION

Typical geochemistry characteristics of scheelite from skarns

Higher Mo content and a negative correlation between MoO_3 and WO_3

Due to their similar electronic configurations, ionic radii and valence states, hexavalent Mo can substitute for W (Mo^{6+} for W^{6+}) in a complete solid solution series from scheelite ($CaWO_4$) to powellite ($CaMoO_4$) (Liu 1987; Raimbault et al. 1993). As a hydrothermal mineral from porphyry-skarn-type W-Mo deposits, scheelite contains high MoO_3 and, because Mo migrates as Mo^{6+} in fluid under oxidized conditions (Rempel et al. 2009), it is likely that W substitution occurred during the oxidation stage. The typical signatures of scheelite from the Baizhangyan and Jitoushan deposits include very high Mo (most > 7,000 ppm, Table 2) and Sr contents (most > 100 ppm, Table 2), but lower concentrations of Cu, Pb, Zn, Sn and Rb (most < 20 ppm, Table 2). Trace element analysis also revealed that all of the scheelite samples had very low concentrations of Fe and Mn. In contrast, scheelite from vein-type Au-W deposits had the lowest Mo contents (0-10 ppm; Fig. 5a). The great contrast in scheelite Mo content is an effective index to distinguish between different types of deposits, and is particularly useful for differentiating skarn-type W-Mo deposits from vein-type Au-W deposits.

FIGURE 5. (a) Comparison of Mo content (ppm) in scheelite from W-Mo-(Sn-Bi) and Au-W deposits. (b) Plot of MoO_3 versus WO_3 in scheelite from W-(Mo) deposits.

Strong HREE depletion

REEs are well-established petrogenetic indicators, particularly in magmatic systems (e.g., Lipin and McKay 1989). They are also commonly used in tracking the fluid sources and chemistry of hydrothermal systems (e.g., see review by Gieré 1996), however, little research has been performed on the REE composition of skarn-type scheelite. In our study, the $LREE/HREE_N$ values of scheelite from the Baizhangyan and Jitoushan deposits ranged from 4.637-648.8, and the majority were between 50 and 300 (Table 3). These results showed that the scheelite from the two skarn deposits had a typical right-dip-type REE_N pattern (Figs. 6, 1-8), enriched in LREE and strongly depleted in HREE with a positive to negative Eu anomaly. Compared with the REE composition of vein-type scheelite (Henderson 1985; Zhang et al. 1990; Raimbault et al. 1993; Sylvester and Ghaderi 1997; Ghaderi et al. 1999; Brugger et al. 2000, 2002, 2008; Dostal et al. 2009; Peng et al. 2010) and porphyry-type scheelite (Zhang et al. 1990), the scheelite samples from the Jitoushan and Baizhangyan deposits were more depleted in HREEs (Fig. 6). The skarn-type scheelite samples had geochemical characteristics that were similar to porphyry-type scheelite (Zhang et al. 1990) (Fig. 7) with right-dip REE patterns. In addition, the scheelite samples from different types of deposits could be well discriminated on a triangular LREE-MREE-HREE diagram (Fig. 7). This suggests that, in addition to Mo content,

scheelite REE patterns can also be used to distinguish different deposit types.

FIGURE 6. Chondrite-normalized REE_N patterns for scheelite samples from the Baizhangyan and Jitoushan deposits. The normalization values were taken from Sun and McDonough (1989). The REE data of the metallogenetic rocks and garnet were taken from Song (2010).

FIGURE 7. Triangular LREE-MREE-HREE diagram of the scheelite from the Baizhangyan and Jitoushan deposits. (The REE data of scheelite from vein-type Au-W, vein-type W and porphyry-type W-Mo deposits were taken from Henderson 1985; Zhang et al. 1990; Raimbault et al. 1993; Sylvester and Ghaderi 1997; Ghaderi et al. 1999; Brugger et al. 2000, 2002, 2008; Dostal et al. 2009 and Peng et al. 2010).

Records of ore-forming fluids

Decoupling between LREEs and HREEs

The temperature, pressure and composition of the hydrothermal fluid, and the nature of the REE speciation in the fluid, all influence the partitioning of the REEs between the scheelite and the fluid (Brugger et al. 2008). As previously noted, there is a scarcity of data on the solubility and partitioning of REEs between hydrothermal fluids and scheelite. Much of the research has assumed that all REEs have similar partition coefficients so the decoupling of LREEs and HREEs within scheelite is one of its most interesting geochemical characteristics. Figure 8 shows positive correlations among LREEs except for Eu, which is susceptible to redox conditions. While the same situation occurs among HREEs in scheelite, there are no correlations between LREEs and HREEs (Fig. 8). Haas et al. (1995) argued that chloride, fluoride and hydroxide complexes are most effective in transporting REEs in acid, neutral and basic solutions, respectively. The available experimental data show that REE complexing (e.g. in chloride and fluoride complexes) in hydrothermal fluids can preferentially stabilize LREEs over HREEs (Flynn and Burnham 1978; Midgisov et al. 2006, 2009). Song (2010) reported that the REE patterns of granodiorite, garnet and limestone from the Jitoushan deposit have right-dip-type REE_N patterns, similar to scheelite REE patterns and Figure 6 shows that garnets are enriched in HREEs relative to scheelite. In this study, the $HREE_N$ content of scheelite is lower than that of granodiorite, garnet and limestone, and scheelite has the highest $LREE/HREE_N$ ratio. Figure 4 shows that the studied Jitoushan and Baizhangyan scheelite precipitated during the oxide stage, following the skarn stage. Several studies have shown that most garnet and amphibole from metamorphic and magmatic systems are HREE enriched and LREE depleted (e.g., Graunch 1989; Bea et al. 1997; Zhang et al. 2000; Boyd et al. 2004). As a result, the precipitation of skarn minerals (e.g., garnet, diopside, amphibole) at Jitoushan and Baizhangyan likely resulted in an enrichment of LREEs and depletion of HREEs in the residual fluids. Scheelite primarily inherits its REE pattern from the ore-forming fluid (Sylvester and Ghaderi 1997; Ghaderi et al. 1999; Brugger et al. 2000; Dostal et al. 2009; Peng et al. 2010), so it is reasonable to suggest that the typical right-dip-type REE_N pattern of the skarn-type scheelite was

controlled by the earlier precipitation of skarn minerals which left the residual fluid depleted in HREEs. (e.g., Graunch 1989; Bea et al. 1997; Zhang et al. 2000; Boyd et al. 2004).

FIGURE 8. Plots of HREEs versus Dy (1-9), LREEs versus Ce (10-13), HREEs versus LREEs (14) and HREEs versus MREE (15) in scheelite from the Baizhangyan and Jitoushan deposits.

Substitution mechanisms of REE^{3+} for Ca^{2+} in skarn-type scheelite

Studies have shown that the REE geochemistry of scheelite is strongly influenced by the charge balance and the crystal structure, particularly the size of the Ca site (Raimbault et al. 1993; Ghaderi et al. 1999). The substitution of trivalent REE for divalent Ca requires a charge-compensating mechanism to maintain electrostatic neutrality. Nassau (1963), Burt (1989) and Ghaderi (1999) presented coupled substitution schemes between REE^{3+} and Ca in scheelite. Of the numerous mechanisms suggested by these authors, the following are considered the most important:

$$2Ca^{2+} = REE^{3+} + Na^{+} \quad (1)$$

$$Ca^{2+} + W^{6+} = REE^{3+} + Nb^{5+} \quad (2)$$

$$3Ca^{2+} = 2REE^{3+} + \square Ca \quad (3)$$

where □Ca is a Ca site vacancy. Different mechanisms by which REE^{3+} substitutes for Ca^{2+} in scheelite result in different REE_N patterns. For example, relatively flat chondrite-normalized REE patterns result from the $3Ca^{2+}=2REE^{3+}+\square Ca$ substitution, whereas the MREE enrichment of the type observed in the Björkdal scheelite arises from the $2Ca^{2+}=REE^{3+}+Na^{+}$ substitution (Ghaderi et al. 1999) and is consistent with the relationship between the Nd/Ca and Na/Ca ratios. However, Brugger et al. (2002, 2008) questioned some of the substitution mechanisms proposed by Ghaderi et al. (1999). It is, therefore, important to identify the mechanisms that explain the REE characteristics of skarn-type scheelite.

If Na is the element providing the charge balance in the studied scheelite samples, then the ionic radius of the REE^{3+} that preferentially substitutes into the Ca site can be calculated from equation (1) (Ghaderi et al. 1999). By extending the compensation hypothesis to both size and charge, we can estimate the ionic radius of the REE^{3+} that preferentially substitutes into the Ca site. Using ionic radii from a study by Shannon (1976) for coordination, Ghaderi et al. (1999) considered that a MREE whose ionic radii is close to 1.06 Å would preferentially substitute into a Ca site. The ore-forming fluid responsible for MREE-rich scheelite would, therefore, be enriched in Na and MREE. Although Brugger et al. (2002) attributed REE uptake in scheelite from hydrothermal gold deposits to be dominated by mechanism (1), based on previous studies and our analysis, W-Mo ore-forming fluids have low salinity (5-8 wt% NaCl equivalency; Song et al. 2010) and the scheelite does not display MREE-rich REE

patterns (Fig. 6). It follows that equation (1) is unlikely to comprise the primary substitution mechanism for REE in the studied scheelite.

Similarly, equation (2) requires that the scheelite be rich in Nb^{5+} and have a Nb content nearly equal to the ΣREEs. The positive correlation of Nb^{5+} and Nd^{3+} (Dostal et al. 2009) suggested that the REE and Nb substitution in scheelite from the Nova Scotia deposits was governed by equation (2). The Baizhangyan and Jitoushan scheelite contains only 1-60 ppm Nb (Table 3), much lower than the ΣREEs (ranging from 100-400 ppm) (Table 3), and no positive correlation between Nb^{5+} and Nd^{3+} was observed. This negates substitution described by equation (2) from being applicable in this case.

Zeng et al. (1998) considered that the REE patterns of scheelite from the Nanyangtian deposit were mainly inherited from ore-forming fluids. Substitution described by equation (3) could explain the scheelite REE patterns observed in this work if scheelite mainly inherits its REE signature from the ore fluid and depletion of HREE resulted from prior precipitation of skarn minerals as discussed in the previous section.

Europium anomaly

The redox conditions in a melt can be estimated by observing the variation in the so-called "europium anomaly," based on the variation in the total Eu relative to the neighboring REEs between the melt and a crystallizing mineral or between co-genetic minerals (Brugger et al. 2008). Because Eu can substitute for Ca in scheelite as either Eu^{3+} or Eu^{2+}, the europium anomaly can be used to estimate the redox conditions of ore-forming fluids (Ghaderi et al. 1999; Brugger et al. 2000, 2002, 2008). A high concentration of Eu^{2+} ($Eu^{3+}<Eu^{2+}$) in a hydrothermal solution results in a positive Eu anomaly in the REE pattern, and a high concentration of Eu^{3+} ($Eu^{3+}>Eu^{2+}$) results in a negative Eu anomaly (Zeng et al. 1998; Ghaderi et al. 1999; Xiong et al. 2006). Ghaderi et al. (1999) suggested that the Eu anomalies in scheelite were inherited from the fluids. Brugger et al. (2000) concluded that changes in the Eu anomaly in a scheelite sample arise due to the smaller partition coefficient of Eu^{2+} relative to Eu^{3+} and not because of changes in the oxidation state of the Eu in the fluid. They go on to suggest that, because Eu^{2+} is preferentially incorporated in scheelite, it becomes depleted in the parent fluid during closed system precipitation, leading to a reduction in the size of the Eu anomaly as precipitation proceeds. Brugger et al. (2008) also pointed out that the change in Eu oxidation state observed in scheelite can be explained by a drop in pH. This drop is caused by the onset of fluid-rock interaction, and is also reflected by small changes in the Nd, Sr and Pb isotopic signatures within single scheelite crystals. Figure 6 (4, 5) shows that positive and negative Eu anomalies were found in the same scheelite sample, indicating that the redox conditions, Eu concentrations and pH of the ore-forming fluids might have been in a state of flux during the mineralization process. For a given concentration of REEs in the ore fluid,

different mineral assemblages can develop as a consequence of different physicochemical conditions. A low f_{O2} and/or high f_{S2} may result in the formation of nearly pure scheelite accompanied by molybdenite, while a high f_{O2} and/or low f_{S2} may prohibit the formation of molybdenite (Hsu and Galli 1973). In this work, the Eu anomalies in the scheelite were not dominantly controlled by the substitution mechanism but were inherited from ore-forming fluids with changing redox conditions, Eu concentrations and pH.

Figure 9 displays the complex correlation between δEu and Mo in the scheelite. There was a negative correlation between the δEu and Mo when δEu>1, and a positive correlation when δEu<1. That is, the Mo entered into the scheelite increasingly under oxidized conditions and maximized at the δEu values of 0.8 to 1. In contrast, under reducing conditions, Mo content of scheelite decreases and Mo precipitates as molybdenite. This is corroborated by the changing valence state of Mo in an evolving ore forming fluid. Mo migrates as Mo^{6+} in H_2MoO_4 (Rempel et al. 2009) and enters into scheelite by substituting for W^{6+} in fluids with δEu<1 (oxidized conditions). With changing redox conditions, more Mo^{6+} is reduced to Mo^{4+} and precipitates as MoS_2 in fluid with δEu>1 (reducing conditions) (Linnen and Williams-Jones 1990; Luo et al. 1991). These results are consistent with the mineralization processes in the Baizhangyan and Jitoushan W-Mo deposits. The scheelite precipitated mainly at the oxide stage (Song 2010) following the skarn stage, and the molybdenite precipitated at the quartz-sulfide stage, mainly under reduction conditions.

FIGURE 9. Plot of δEu versus Mo (ppm) in scheelite from the Baizhangyan and Jitoushan deposits.

Constraints on the source

The isotope data from the scheelite can shed some light on the source of the ore-forming fluids associated with mineralization (Bell et al. 1989). Based on the Sr-Nd isotopic analyses of scheelite from different deposits, scheelite from skarn-type W-Mo, vein-type Au (W) and vein-type W (Sb-Au) deposits are easily distinguished. Figure 10 shows that the scheelite sample from vein-type Au (W) deposits plots close to depleted mantle (DM), while the scheelite sample from skarn-type W-Mo deposits plots closer to the lower crust (LC) and upper crust (UC) and the scheelite sample from the vein-type W (Sb-Au) deposits plots closest to the range of UC.

FIGURE 10. $^{143}Nd/^{144}Nd(t)$ versus $^{87}Sr/^{86}Sr(t)$ correlation diagram for scheelite from the skarn-type and vein-type deposits (original plot after Eichhorn et al. 1997; Voicu et al. 2000). DM=depleted mantle (after Song and Frey 1989), UC=upper crust, LC=lower crust (after Jahn et al. 1999). (The Sr-Nd isotope data of scheelite from vein-type Au-W, and vein-type W deposits were taken from Bell et al. 1989; Kent et al. 1995; Darbyshire et al. 1996; Eichhorn et al. 1997; Voicu et al. 2000; Kempe et al. 2001; Brugger et al. 2002; Peng et al. 2006; Xiong et al. 2006 and Peng et al. 2008; Billmström et al. 2009).

The scheelite samples from the vein-type Au (W) deposits had the lowest isotope values of ($^{87}Sr/^{86}Sr$)(t) (most < 0.707) and the highest values of ($^{143}Nd/^{144}Nd$)(t) (with most > 0.5125) (Fig. 10 and Table 4). Many studies have shown that the Sr-Nd isotope values of scheelite from vein-type Au (W) deposits have similar isotopic signatures (Bell et al. 1989; Mueller et al. 1991; Kent et al. 1995; Anglin et al. 1996; Brugger et al. 2002; Robert et al. 2006; Billmström et al. 2009) (Fig. 10). For example, the isotopic signature at Omai (Guyana) is similar to that observed in scheelite from the Mount Charlotte deposit (Australia) (Kent et al. 1995) and the Val d'Or gold camp (Canada) (Anglin et al. 1996). The $^{143}Nd/^{144}Nd$(t) versus $^{87}Sr/^{86}Sr$(t) diagram (Fig. 10) of the Omai scheelite reveals that the most radiogenic Nd compositions fit in the range of the mantle array (e.g., Eichhorn et al. 1997). An isotope study of scheelite from Au-(W) deposits located in the Hollinger-Mclntyre-Coniaurum area in Canada indicated that the Nd and Sr in the fluids were derived from a source with chemical characteristics normally associated with mantle-derived materials (Bell et al. 1989). The gold-bearing hydrothermal fluids were generated during the granulitization of the lower sialic crust, caused by an influx of heat and carbon dioxide from the mantle during late Archean cratonization (e.g., Mueller et al. 1991). These isotopic studies suggested that the hydrothermal fluids responsible for the precipitation of scheelite from vein-type Au (W) deposits were mainly derived from the mantle and reflected only a small contribution from crustal sources (Gibbs and Barron 1983; Gruau et al. 1985; Gibbs 1987; Kent et al. 1995; Anglin et al. 1996; Xiong et al. 2006).

The scheelite from vein-type W (Sb-Au) deposits have the highest ($^{87}Sr/^{86}Sr$)(t) values (most > 0.710) and intermediate ($^{143}Nd/^{144}Nd$)(t) signatures (most between 0.512 and 0.513) (Fig. 10 and Table 4). The Sr-Nd isotopic results indicate that ore-forming fluids have a UC signature. Scheelite studies have shown that the ore-forming fluids in the Woxi W-Sb-Au and Zhazixi W-Sb deposits in West Hunan, China have isotopic signatures that are similar to that of the underlying basement (Peng et al. 2006; Peng et al. 2008). Therefore, ore-forming fluids may include mixtures of source fluids such as fluid from the ancient continental crust beneath the host rock (the Banxi Group), fluid from deep granitoid magmas and fluid from the host rock.

Compared with the scheelite from the vein-type Au-(W) and W-(Sb-Au) deposits, the scheelite from the skarn-type W-Mo deposits had the lowest ($^{143}Nd/^{144}Nd$)(t) values of (most < 0.5125) and intermediate values of ($^{87}Sr/^{86}Sr$)(t) (most between 0.708 and 0.715) (Fig. 10 and Table 4). The εNd(t) values of the scheelite varied from (-16 to -12.3) in the Baizhangyan deposit and from -9.5 to -9.1 in the Jitoushan deposit. Such negative values indicate that the Nd was derived from a source with an Sm/Nd ratio lower than CHUR, a chemical characteristic normally associated with LC-derived materials. The Sr-Nd isotope signature of the scheelite from the Jitoushan

W-Mo deposit was similar to that of the ore-bearing wall rock (Fig. 10). Figure 8 shows that the ($^{143}Nd/^{144}Nd$)(t) and ($^{87}Sr/^{86}Sr$)(t) values for the scheelite from the Baizhangyan deposit were close to the range of isotope values for the scheelite and ore-bearing wall rock from the Jitoushan deposit. This indicates that the ore-forming materials in the Jitoushan and Baizhangyan W-Mo deposits were mainly derived from crustal material (Fig. 10).

IMPLICATIONS

The major elements, trace elements, and REEs of scheelite from the Baizhangyan and Jitoushan skarn-type W-Mo deposits reveal that the precipitation of skarn minerals (e.g., garnet, diopside and amphibole) will result in a strong HREE depletion and the decoupling of LREEs and HREEs with the evolution of ore-forming fluids, and the mechanism responsible for REE substitution by Ca^{2+} in scheelite is $3Ca^{2+}=2REE^{3+}+\square Ca$ (where $\square Ca$ is a Ca site vacancy). It indicates that the scheelites primarily inherit their REE patterns from the ore-forming fluid, and the REE characteristics could be used to constrain the fluid evolution of skarn-type W-Mo deposits. Furthermore, the complex δEu/Mo correlation reveals that Mo entered into the scheelite increasingly under oxidized conditions and maximized when the δEu ranged between 0.8 and 1; In contrast, under reducing conditions, Mo decreases in scheelite as Mo changed valence state and precipitated as molybdenite. The scheelite's Sr-Nd isotopic compositions show that the ore-forming materials in the Jitoushan and Baizhangyan W-Mo deposits are mainly derived from crustal sources. So, it is reasonable to suggest that the scheelite will provide important reference meaning to the genesis research and ore prospecting of skarn-type W-Mo deposits, especially to the deposits which located in the newly found Mo-W-Pb-Zn belt in the south of the YVMB.

Our studies also reveal that the great contrast of Mo content, REE patterns, δEu values and Sr-Nd isotopes in scheelite are very effective indexes to distinguish skarn-type W-Mo deposits, porphyry-type W-Mo deposits and vein-type Au-W deposits. So, studies on scheelite will greatly help us to ascertain the genetic types of mineral deposits, discover the ore guide of prospecting, and evaluate the foreground of prospecting during the geological prospecting processes.

ACKNOWLEDGEMENTS

This study was supported by the Knowledge Innovation Project of the Chinese Academy of Sciences (grant No. KZCX1-YW-15-3) and the NSFC (grant No.41102046). We would like to thank Academician Chang Yinfo for his kind guidance. We also thank the solid isotope laboratory, the Institute of Geology and Geophysics, the Chinese Academy of Sciences, the Key Laboratory of Geological Processes and Mineral Resources, the China University of Geosciences, and the

Anhui Zhongke Mining Co., Ltd. for their kind support in the fieldwork for this study. We would like to thank the reviewers who gave their precious time, tolerance and considered responses to the paper.

REFERENCES CITED:

Allen, C.C., and Folinsbee, R.E. (1944) Scheelite veins related to porphyry intrusives, Hollinger Mine. Economic Geology, 39, 340-348.

Anglin C.D., Jonasson I.R., and Franklin J.M. (1996) Sm-Nd Dating of Scheelite and Tourmaline: Implications for the Genesis of Archcan Gold deposits, Vald'Or, Canada. Economic Geology, 91, 1372-1382.

Bea, F., Montero, P., Garuti, G., and Zacharini, F. (1997) Pressure depende of rare earth element distribution in amphibolite and granulite-grade garnets: A LA-ICP-MS study. Geostandard Newslett, 21, 253-270.

Bell, K., Anglin, C.D., and Franklin, J.M. (1989) Sm-Nd and Rb-Sr isotope systematics of scheelites: Possible implications for the age and genesis of vein-hosted gold deposits. Geology, 17, 500-504.

Billmström, K., Broman, C., Jonsson, E., Recio, C., Boyce, A.J., and Torssander, P. (2009) Geochronological, stable isotopes and fluid inclusion constraints for a premetamorphic development of the intrusive-hosted Bjo¨rkdal Au deposit, northern Sweden. International Journal of Earth Science, 98, 1027-1052.

Boyd, F.R., Pearson, D.G., Hoal, K.O., Hoal, B.G., Nixon, P.H., Kingston, M.J., and Mertzman, S.A. (2004) Garnet lherzolites from Louwrensia, Namibia: bulk composition and P/T relations. Lithos, 77, 573-592.

Brugger, J., Bettiol, A., Costa, S., Lahaye, Y., Bateman, R., Lambert, D., and Jamieson, D. (2000) Mapping REE distribution in scheelite using luminescence. Mineralogical Magazine, 64, 891-903.

Brugger, J., Etschmann, B., Pownceby, M., Liu, W., Grundler, P., and Brewe, D. (2008) Oxidation state of europium in scheelite: Tracking fluid-rock interaction in gold deposits. Chemical Geology, 257, 26-33,

Brugger, J., Mass, R., Lahaye, Y., Mcrae, C., Ghaderi, M., Costa, S., Lambert, D., Bateman, R., and Prince, K. (2002) Origins of Nd-Sr-Pb isotopic variations in single scheelite grains from Archaean gold deposits, Western Australia. Chemical Geology, 182, 203-225.

Burt, D.M. (1989) Compositional andd phase relations among rare earth elements. Reviews in Mineralogy. 21, 259-307.

Byrne, R.H., and Li, B. (1995) Comparative complexation behavior of the rare earths. Geochimica et Cosmochimica Acta, 59, 4575-4589.

Chang, Y.F., Liu, X.P., and Wu, C.Y. (1991) The copper-iron belt of the Lower and Middle Reaches of the Changjiang River, 391 p. Geological Publishing House, Beijing.

Chen, B.C. (1986) Research on scheelite from Yangchuling porphyry type W-Mo deposit. Geology and Prospecting, 22,35-40.

Chu, Z.Y., Chen, F.K., Yang, Y.H., and Guo, J.H. (2009) Precise determination of Sm, Nd concentrations and Nd isotopic compositions at the nanogram level in geological samples by thermal ionization mass spectrometry. Journal of Analytical Atomic Spectrometry, 24, 1534-1544.

Chu, Z.Y., Guo, J.H., Yang, Y.H., Qi, L., Chen, L., Li, X.C., and Gao, J.F. (2012) Evaluation of sample dissolution method for Sm-Nd isotopic analysis of scheelite. Journal of Analytical Atomic Spectrometry, 27, 509-515.

Cottrant, J.F. (1981) Cristallochimie et géochimie des terres rares dans la scheelite: application à quelques gisements francçais. Ph.D. thesis, University of Paris-VI, France.

Darbyshire, D.P.F., Pitfield, P.E.J, and Campbell, S.D.G. (1996) Late Archean and Early Proterozoic gold-tungsten mineralization in the Zimbabwe Archean craton: Rb-Sr and Sm-Nd isotope constraints. Geology, 24, 19-22.

Deer, W.A., Howie, R.A., and Zussman, J. (1966) An introduction to the Rock Forming Minerals, 515 p. Longman Press, New York.

Dostal, J., Kontak, D.J., and Chatterjee, A. (2009) Trace element geochemistry of scheelite and rutile from metaturbidite-hosted quartz vein gold deposits, Meguma Terrane, Nova Scotia, Canada: genetic implications. Mineralogy and Petrology, 97, 95-109.

Eggins, S.M., Kinsley, L.P.J., and Shelley, J.M.G. (1998) Deposition and element fractionation processes during atmospheric pressure laser sampling for analysis by ICP-MS. Applied Surface Science, 129, 278-286.

Eichhorn, R., Hll, R., Jagoutz, E., and Schrer, U. (1997) Dating scheelite stages: A strontium, neodymium, lead approach from the Felbertal tungsten deposit, Central Alps, Austria. Geochimica et Cosmochimica Acta, 61, 5005-5022.

Flynn, R.T., and Burnham, C.W. (1978) An experimental determination of rare earth element partition coefficients between a chloride containing vapour phase and a silicate melt. Geochimica et Cosmochimica. Acta, 42, 685-701.

Ghaderi, M. (1998) Sources of Archaean gold mineralization in the Kalgoorlie-Norseman region of Western Australia, determined from strontium-neodymium isotopes and trace elements in scheelite and host rocks, 231 p. Ph.D. thesis, the Australian National University Canberra, Australia.

Ghaderi, M., Palin, J.M., Campbell, I.H., and Sylvester, P.J. (1999) Rare earth element systematics in scheelite from hydrothermal gold deposits in the Kalgoorlie-Norseman region, Western Australia. Economic Geology, 94, 423-437.

Gibbs, A.K. (1987) Proterozoic volcanic rocks of the northern Guyana Shield, South America. In T.C. Pharaoh and R.D. Beckinsale, Eds., Geochemistry and mineralisation of Proterozoic volcanic suites, p. 275-288. Geological Society of London, Special Publication 33 Blackwell, Oxford.

Gibbs, A.K., and Barron, C.N. (1983) The Guiana Shield reviewed. Episodes, 2, 7-14.

Graunch, R.I. (1989) Rare earth elements in metamorphic rocks in Geochemistry and Mineralogical Rare Earth Elements. In B.R. Lipin and G.A. Mckay, Eds., Review Mineral, 21, p. 146-167. Mineralogical Society of America.

Gruau, G., Martin, H., Leveque, B., and Capdevilla, R. (1985) Rb-Sr and Sm-Nd geochronology of Lower Proterozoic granite-greenstone terrains in French Guiana, South America. Precambrian Research, 30, 63-80.

Günther, D., and Heinrich, C.A. (1999) Comparison of the ablation behaviour of 266 nm Nd:YAG and 193 nm ArF excimer lasers for LA-ICP-MS analysis. Journal of Analytical Atomic Spectrometry, 14, 1369-1374.

HaasJ, R., Shock, E.L., and Sassani, D.C., (1995) Rare earth elements in hydrothermal systems: Estimates of standard partial molar thermodynamic properties of aqueous complexes of rare earth elements at high pressure and temperature. Geochimica et Cosmochimica Act, 59, 4329-4350.

Henderson, P. (1985) Crystal chemistry and geochemistry of some mineral crystal. Geology Geochemistry Supplement, 1-4.

Hu, S.X., Sun, M.Z., Ren, Q.j., and Zheng, S.J. (1977) The alkali metasomatism of iron, copper deposits and the metallogenetic specialization about igneous rocks in the lower-middle Yangtze Valley mineralization belt. Journal of Nanjing University, 2, 91-112.

Ishihara, S., Li, W.D., Sasaki, A., Shibata, K., Matsuhisa, Y., and Terashima, S. (1986) Characteristics of Cretaceous magmatism and related mineralization of the Ningwu Basin, Lower Yangtze area, eastern China. Bulletin Geological Survey of Japan, 37, 207-231.

Jahn, B., Wu, F., Lo, C., and Tsai, C. (1999) Crust-mantle interaction induced by deep subduction of the continental crust: geochemical and Sr-Nd isotopic evidence from post-collisional mafic-ultramafic intrusions of the northern Dabie complex, central China. Chemical Geology, 157, 119-146.

Jiang, Q.S., Yu, C.Z., Huang, and W.P. (2009) Geological features and ore-control factors of the Gaojiabang tungsten ore deposit, Qingyang County, Anhui Province . Geol Anhui, 19, 251-254.

Kempe, U., Belyatsky, B., Krymsky, R., Kremenetsky, A., and Ivanov, P.A. (2001) Sm-Nd and Sr isotope systematics of scheelite from the giant Au (-W) deposit Muruntau (Uzbekistan): implications for the age and sources of Au mineralization. Mineralium Deposita, 36, 379-392.

Kent, A.J.R., Campbell, I.H., and McCulloch, M.T. (1995) Sm-Nd systematics of hydrothermal scheelite from the Mount Charlotte mine, Kalgoorlie, Western Australia: an isotopic link between gold mineralization and komatiites. Economic Geology, 90, 2329-2335.

Li, Q.L., Chen, F., Wang, X.L., Li, X.H., and Li, C.F. (2005) Low-blank chemical separation procedure and the single grain mica Rb-Sr isochron dating method. Chinese Science Bulletion, 50, 2861-2865.

Li, S.G. (2001) Infrastructure of Mesozoic magmatic rocks and copper-iron metallogenetic belt in the middle and lower Yangtze River reaches. Geology of Anhui, 11, 118-123.

Linnen, R.L. and Williams-Jones, A.E. (1990) Evolution of aqueous-carbonic fluids during contact metamorphism, wallrock alteration, and molybdenite deposition at Trout Lake, British Columbia. Econ. Geol., 85, 1840-1856.

Liu, Y., Deng, J., Li, C.F., Shi, G.H., and Zheng, A.L. (2007) REE Geochemistry and Sm-Nd Isotopic Dating of Scheelite from Xuebaoding Mine in Sichuan. Chinese Science Bulletion, 52, 1923-1929.

Liu, Y.J., and Ma, D.S. (1987) Geochemistry of Tungsten, 217 p. Science Press, Beijing.

Liu, Y.J., Zhang, J.R. and Chen, J. (1983) Mineralology and occurrence states of ore-forming elements of Shizuyuan W-Mo-Bi-Sn deposit. Geological Review, 29, 255-264.

Luo, M.J., Zhang, F.M., and Dong, Q.Y. (1991) Chinese Molybdenum Deposit, 425 p. Henan Science and Technology Press, Zhengzhou.

Mao, J.W., Zhang, Z.H., Yu, J.J., Wang, Y.T., and Niu, B.G. (2003) The geodynamics setting of large-scale ore-forming in Mesozoic in North China: From the precision age of metal deposits. Science in China, Series D, 33, 289-300.

Migdisov, A. A., Reukov, V. V., and Williams-Jones, A. E. (2006) A spectrophotometric study of neodymium (III) complexation in sulfate solutions at elevated temperatures. Geochimica et Cosmochimica Acta, 70, 983-992.

Migdisov, A. A., Williams-Jones, A. E., and Wagner, T. (2009) An experimental study of the solubility and speciation of the Rare Earth Elements (III) in fluoride- and chloridebearing aqueous solutions at temperatures up to 300 degrees C. Geochimica et Cosmochimica Acta, 73, 7087-7109.

Mueller, A.G., Laeter J.R.D., David I., and Groves D.I. (1991) Strontium Isotope Systematics of Hydrothermal Minerals from Epigenetic Archean Gold Deposits in the Yilgarn Block, Western Australia. Economic Geology, 86, 780-809.

Nassau, K., and Loiacono, G.M. (1963) Calciumt ungstate-III: Trivalent rare earths ubstitution. Journal of Physics and Chemistry of Solids. 24, 1503-1510.

Noble, S., Spooner E.T.C., and Harris F. (1984) The Logtung large tonnage, low-grade W (scheelite)-Mo porphyry deposit, south-central Yukon Territory. Economic Geology, 79, 848-868.

Peng, B., Frei R., and Tu X.L. (2006) Nd-Sr-Pb Isotopic Geochemistry of Scheel ite from the W oxi W-Sb-Au Deposit，W estern Hunan：Impl ications for Sources and Evol ution of Ore-forming Fluids. Acta Geological Sinica, 80, 561-570.

Peng, J.T., Hu, R.Z., Zhao, J.H., and Fu, Y.Z. (2003) Scheelite Sm-Nd dating and quartz Ar-Ar dating from W oxi Au-Sb-W deposit western Hunan. Chinese Science Bul1etin, 48, 2640-2646.

Peng, J.T., Zhang, D.L., Hu, R.Z., Wu, M.J., and Lin, Y.X. (2008) Sm-Nd and Sr Isotope Geochemistry of Hydrothermal Scheelite from the Zhazixi W-Sb Deposit,Western Hunan. Acta Geological Sinica, 82, 1514-1521.

Peng, J.T., Zhang, D.L., Hu, R.Z., Wu, M.J., Liu, X.M., Qi, L., and Yu, Y.L. (2010) Inhomogeneous Distribution of Rare Earth Elements (REEs) in Scheelite from the Zhazixi W-Sb Deposit, Western Hunan and Its Geological Implications. Geological Review, 56, 810-819.

Qin, K.Z., Wang, D.P., Wang, Z.T., and Sun, S. (1999) Types, geological background, metallogenic provinces and ore-forming systematics of major copper deposits in Eastern China. Mineral Deposits, 18, 359-371.

Qin, Y., Wang, D.H., Wu, L.B., Wang K,.Y., Mei, Y.P. (2010) Zircon SHRIMP U-Pb dating of the mineralized porphyry in the Dongyuan W deposit in Anhui Province and its geological significance. Acta Geological Sinica, 84, 479-484.

Raimbault, L., Baumer, A., Dubru, M., Benkerrou, C., Croze, V., and Zahm, A. (1993) REE fractionation between scheelite and apatite in hydrothermal conditions. American Mineralogist, 78, 1275-1285.

Rempel, K.U., Williams-Jones, A.E., and Migdisov, A.A. (2009) The partitioning of molybdenum (VI) between aqueous liquid and vapour at temperatures up to 370 C. Geochimica et Cosmochimica Acta, 73(11): 3381-3392.

Roberts, S., Palmer, M.R., and Waller, L. (2006) Sm-Nd and REE characteristics of tourmaline and scheelite from the Bjorkdal gold deposit, northern Sweden: evidence of an intrusion-related gold deposit? Economic Geology, 101, 1415-1425.

Rosing, M.T. (1990) The theoretical effect of metasomatismon Sm-Nd isotopic systems. Geochimica et Cosmochimica Acta, 54, 1337-1341.

Shannon, R.D. (1976) Revised effective ionic radii and systematic studies of interatomic distances in halides and chalcogenides. Acta Crystallographica. 32, 751-767.

Song, G.X. (2010) Research on Magmatism-Mineralization and Metallogenic system of skarn-porphyry type W-Mo deposits in Chizhou area, the Middle-Lower Yangtze Valley, 151 p. Ph.D. thesis. Institute of Geology and Geophysics, Chinese Academy of Science, China.

Song, G.X., Qin, K.Z., and Li, G.M. (2008) Types, temporal and spatial distribution of molybdenum deposits and discussion of their dynamics setting in the Lower-Middle Yangtze Valley. 9th National deposits conference Paper Collection, p. 27-28. Geological Publishing House, Beijing.

Song, G.X., Qin, K.Z., and Li, G.M. (2010) Study on the fluid inclusions and S-H-O isotopic compositions of skarn-porphyry-type W-Mo deposits in Chizhou area in the Middle-Lower Yangtze Valley. Acta Petrologica Sinica, 26, 2768-2782.

Song, G.X., Qin, K.Z., Li, G.M., Li, X.H. and Qu, W.J. (2013) Intrusive-Mineralization Ages and Ore-Forming Fluids of the Baizhangyan W-Mo Deposit in Chizhou Area, the Middle-Lower Yangtze Valley, SE-China. Resource Geology, 63(1), 57-71.

Song, G.X., Qin, K.Z., Li, G.M., Li, X.H., Li, J.X., Liu, T.B., and Chang, Z.S. (2012) Geochronologic and isotope geochemical constraints on magmatism and associated W-Mo mineralization of the Jitoushan W-Mo deposit, middle-lower Yangtze Valley. International of Geological Review, 54, 1532-1547.

Song, Y., and Frey, F.A. (1989) Geochemistry of peridotite xenoliths in basalt from Hannuoba, Eastern China: Implications for subcontinental mantle eterogeneity. Geochimica et Cosmochimica Acta, 53, 97-113.

Sun, S.S., and McDonough, W.F. (1989) Chemical and isotopic systematics of oceanic basalts: implications for mantle composition and processes. In A.D. Saunders and M.J. Norry, Eds., Magmatism in the Ocean Basins. Special Publication 42, p. 313-345. Geological Society of London, London.

Sylvester, P.J., and Ghaderi, M. (1997) Trace element analysis of scheelite by excimer laser ablation inductively coupled plasma mass spectrometry (ELA-ICP-MS) using a synthetic silicate glass standard. Chemical Geology, 141, 49-65.

Tomschi, H.P., Oberthür, T., Saager, R., and Kramers, J. (1986) Geochemical and mineralogical data on the genesis of the Mazowe gold field in the Harare-Bindura greenstone belt, Zimbabwe. Geocongress'86, Ext Abstr vol, 345-348.

Uspensky, E., Brugger, J. and Graeser, S. (1998) REE geochemistry systematics of scheelite from the Alps using luminescence spectroscopy: from global regularities to local control. Schweizerische Mineralogische und Petrographische Mitteilungen, 78, 33-56.

Voicu, G., Bardoux, M., Stevenson, R., and Jebrak, M. (2000) Nd and Sr isotope study of hydrothermal scheelite and host rocks at Omai, Guiana Shield: implications for ore fluid source and flow path during the formation of orogenic gold deposits. Mineralium Deposita, 35, 302-314.

Wang, R.C., Zhu, J.C., Zhang, W.L., Xie, L., Yu, A.P., and Che, X.D. (2008) Ore-Forming Mineralogy of W-Sn Granites in the Nanling Range:Concept and Case Study. Geological Journal of China Universities, 14, 485-495.

Wang, X.D., Wang, X.W., and Sun, C.M. (2010) REE Geochemistry of Scheelite and Sm-Nd Dating for the Houchangchuan Scheelite Deposit in Gansu. Journal of Mineralogy Petrology, 30, 64-68.

Wang, Z.T., and Qin, K.Z. (1989) Types, metallogenic environments and characteristics of temporal and spatial distribution of copper deposits in China. Acta Geological Sinicaica, 2, 79-92.

Xiong, D.X., Sun, X.M., Shi, G.Y., Wang, S.W., Gao, J.F., and Xue, T. (2006) Trace elements, rare earth elements (REE)and Nd-Sr isotopic compositions in scheelites and their implications for the nfineralization in Daping gold mine in Yunnan province, China. Acta Petrologica Sinica, 22, 733-741.

Xu, K.Q. (1957) Finding of skzrn Ca-W deposit in Yaogangxian W-Mn-Fe mine in Hunan Province and the genesis relation between the two kinds of deposits. Acta Geological Sinicaica, 2, 117-151.

Zeng, Z.G, Li, C.Y., Liu, Y.P., and Tu, G.Z. (1998) REE Geochemistry of scheelite of two genetic types from Nanyangtian, Southeastearn Yunnan. Geology-Geochemistry, 26, 34-38.

Zhai, Y.S., Yao, S.Z., Lin, X.D., and Zhou, X.R. (1992) Fe-Cu (Au) Metallogeny of the Middle-Lower Changjiang Region, 235 p. Geological Publishing House, Beijing.

Zhang, .Y.X. (1982) Geology and Geochemical characters of Yangchuling porphyry type W-Mo deposit and discussion on ore gensis.Geochemistry, 2, 122-132.

Zhang, H., Menzies, M.A., Lu, F., and Zhou, X. (2000) Major and trace element studies on garnets from Paleozoic kimberliteborne mantle xenoliths and megacrysts from the North China craton. Science China D, 43, 423-430.

Zhang, J.J., Mei, Y.P., Wang, D.H., and Li, H.Q. (2008) Isochronology Study on the Xianglushan Scheelite Deposit in North Jiangxi Province and Its Geological Significance. Acta Geological Sinica, 82, 927-931.

Zhang, Y.X., Liu, Y.M., Gao, S.D., and He, Q.G. (1990) Earth elements geochemical characteristics of tungstenic minerals: A distinguishing sign for ore-forming type. Geochemica, 19, 11-20.

Zhao, K.D., and Jiang, S.Y. (2004) Direct Isotope Dating for Metallic Ore Deposits. Earth Science Frontiers, 11, 425-433.

Zhou, T.F., Fan, Y., and Yuan, F. (2008) Advances on petrogenesis and metallogeny study of the mineralization belt of the Middle and Lower Reaches of the Yangtze River area. Acta Petrologica Sinica, 24, 1666-1678.

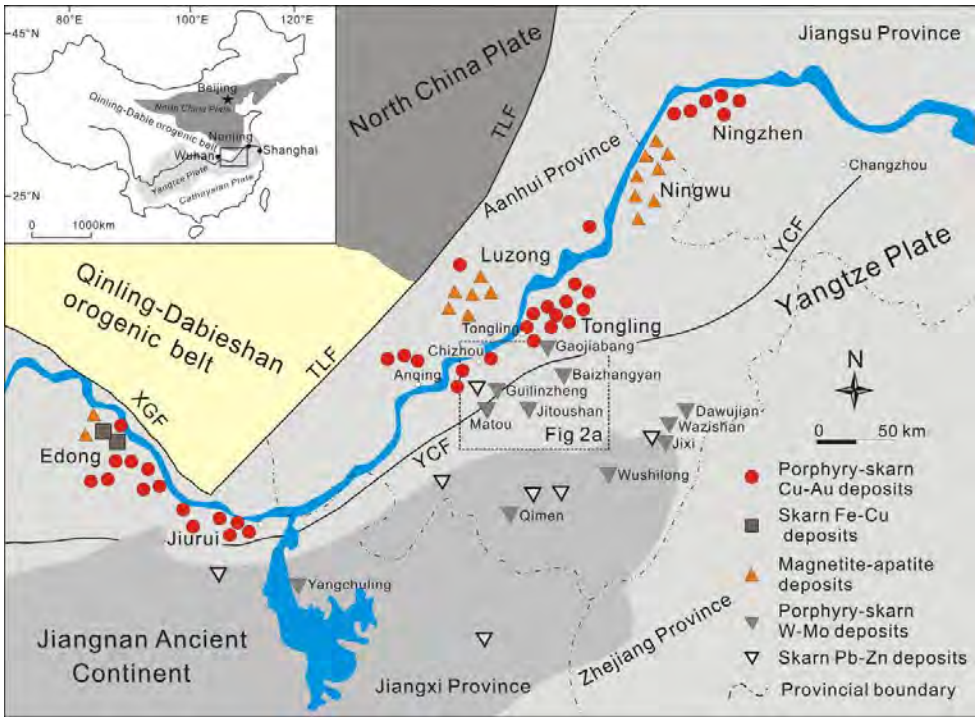
80°E
100°E
120°E
45°N
25°N
0
1000km
Beijing
North China Plate
Qinling-Dabie orogenic belt
Nanjing
Wuhan
Shanghai
Yangtze Plate
Cathaysian Plate
North China Plate
TLF
Jiangsu Province
Aanhui Province
Ningzhen
Ningwu
Changzhou
YCF
Yangtze Plate
Luzong
Tongling
Tongling
Gaojiabang
Chizhou
Anqing
Baizhangyan
Guilinzheng
Jitoushan
Matou
Fig 2a
Dawujian
Wazishan
Jixi
Qinling-Dabieshan orogenic belt
TLF
XGF
Edong
YCF
Wushilong
Qimen
Jiurui
Yangchuling
Jiangnan Ancient Continent
Jiangxi Province
Zhejiang Province
N
0
50 km
Porphyry-skarn Cu-Au deposits
Skarn Fe-Cu deposits
Magnetite-apatite deposits
Porphyry-skarn W-Mo deposits
Skarn Pb-Zn deposits
Provincial boundary

FIGURE. 1

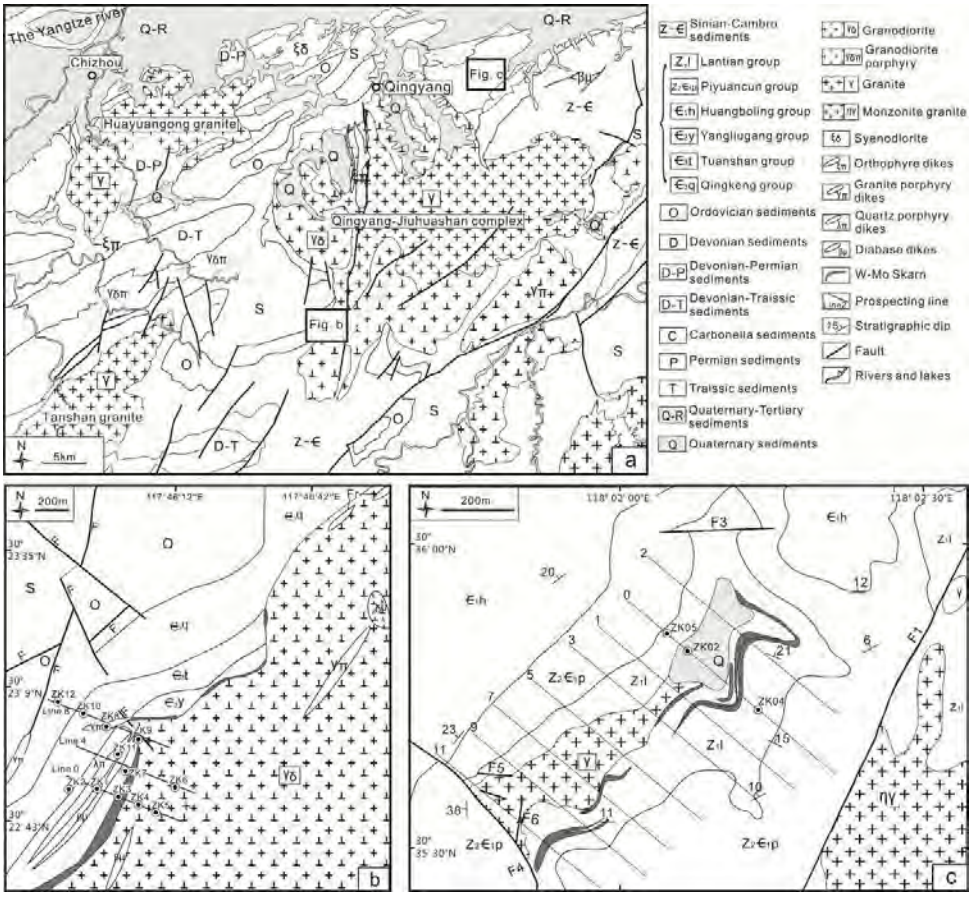
The Yangtze river
Chizhou
Qingyang
Huayuangong granite
Tanshan granite
Qingyang-Jiuhuashan complex
Fig. b
Fig. c
5km
a
Z-∈ Sinian-Cambro sediments
Z₂l Lantian group
Z₂∈₁q Piyuancun group
∈₁h Huangboling group
∈₁y Yangliugang group
∈₁t Tuanshan group
∈₁q Qingkeng group
O Ordovician sediments
D Devonian sediments
D-P Devonian-Permian sediments
D-T Devonian-Traissic sediments
C Carbonella sediments
P Permian sediments
T Traissic sediments
Q-R Quaternary-Tertiary sediments
Q Quaternary sediments
γδ Granodiorite
γδπ Granodiorite porphyry
γ Granite
ηγ Monzonite granite
ξδ Syenodiorite
δμ Orthophyre dikes
γπ Granite porphyry dikes
Qπ Quartz porphyry dikes
μβ Diabase dikes
W-Mo Skarn
Prospecting line
Stratigraphic dip
Fault
Rivers and lakes
200m
b
c
F1
F3
F5
F6
ZK01
ZK02
ZK03
ZK04
ZK05
ZK06
ZK07
ZK08
ZK09
ZK10
ZK11
ZK12

FIGURE. 2

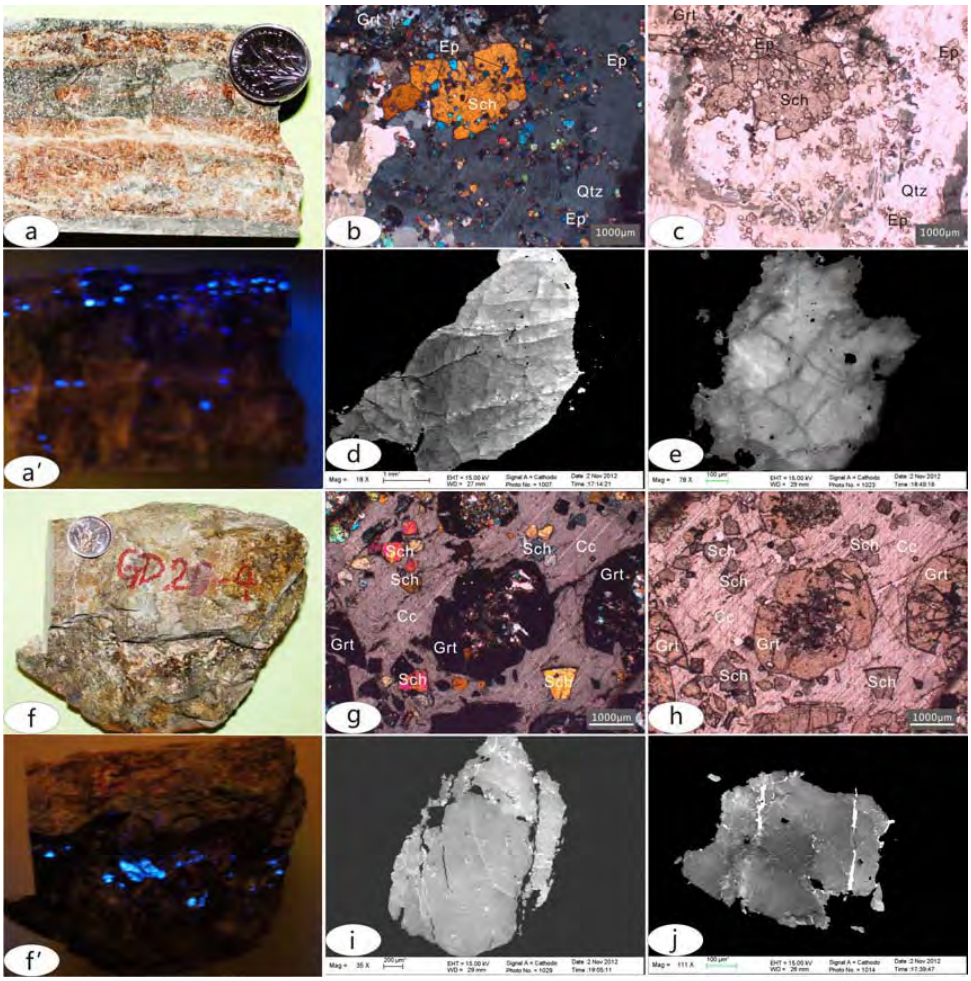
a
b
Grt
Ep
Ep
Sch
Qtz
Ep
1000μm
c
Grt
Ep
Ep
Sch
Qtz
Ep
1000μm
a′
d
e
f
GD2
g
Sch
Sch
Cc
Grt
Sch
Cc
Grt
Grt
Sch
Sch
1000μm
h
Sch
Sch
Cc
Grt
Sch
Cc
Grt
Grt
Sch
Sch
1000μm
f′
i
j

FIGURE. 3

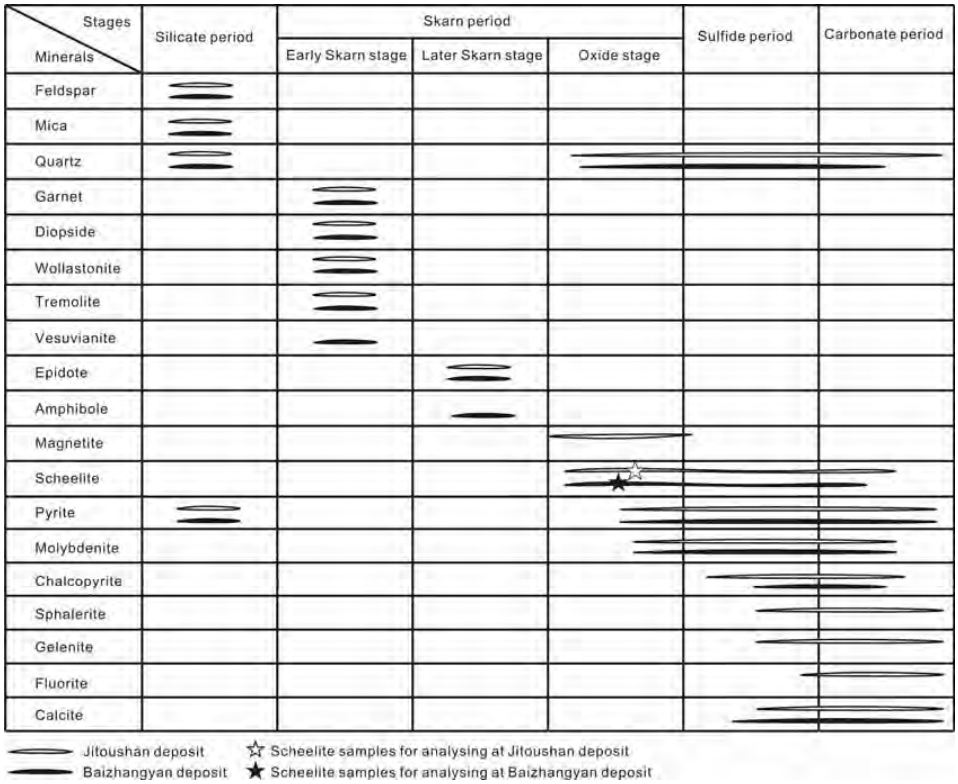
Stages
Minerals
Silicate period
Skarn period
Early Skarn stage
Later Skarn stage
Oxide stage
Sulfide period
Carbonate period
Feldspar
Mica
Quartz
Garnet
Diopside
Wollastonite
Tremolite
Vesuvianite
Epidote
Amphibole
Magnetite
Scheelite
Pyrite
Molybdenite
Chalcopyrite
Sphalerite
Gelenite
Fluorite
Calcite
Jitoushan deposit
Baizhangyan deposit
Scheelite samples for analysing at Jitoushan deposit
Scheelite samples for analysing at Baizhangyan deposit

FIGURE.4

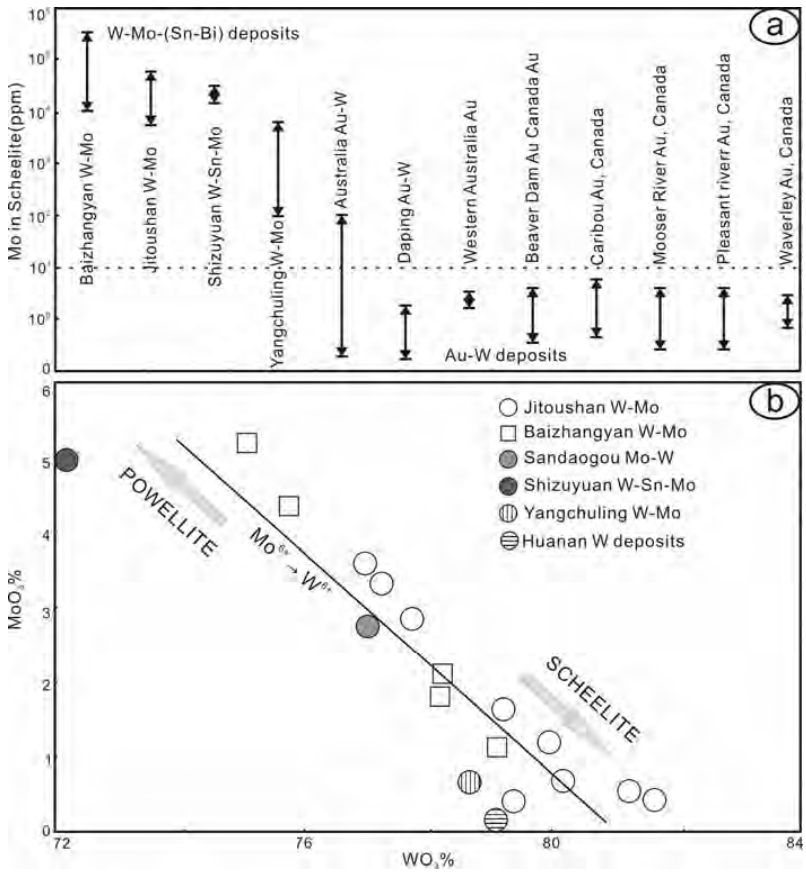
a
W-Mo-(Sn-Bi) deposits
Mo in Scheelite(ppm)
Baizhangyan W-Mo
Jitoushan W-Mo
Shizuyuan W-Sn-Mo
Yangchuling W-Mo
Australia Au-W
Daping Au-W
Western Australia Au
Beaver Dam Au Canada Au
Caribou Au, Canada
Mooser River Au, Canada
Pleasant riverr Au, Canada
Waverley Au, Canada
Au-W deposits
b
Jitoushan W-Mo
Baizhangyan W-Mo
Sandaogou Mo-W
Shizuyuan W-Sn-Mo
Yangchuling W-Mo
Huanan W deposits
POWELLITE
SCHEELITE
MoO3%
WO3%
72
76
80
84

FIGURE. 5

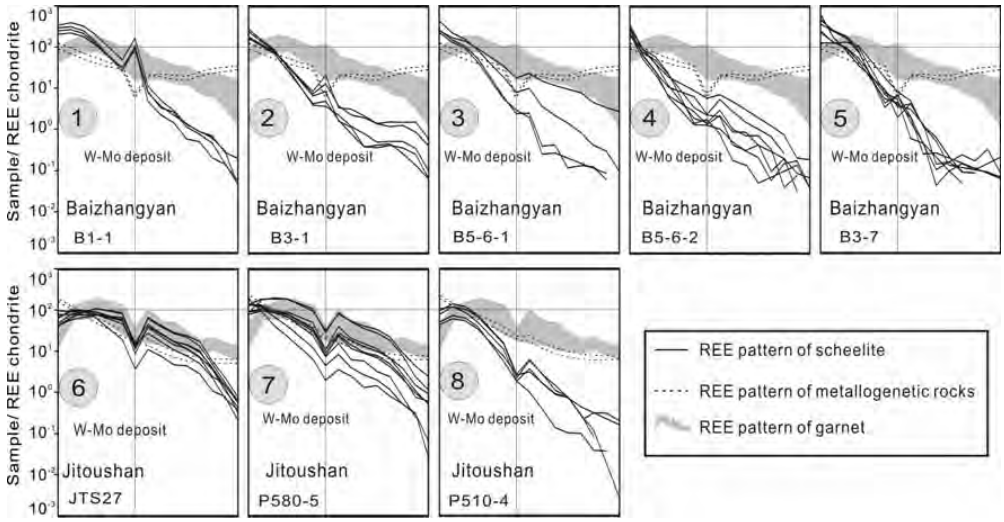
Sample/ REE chondrite
1
W-Mo deposit
Baizhangyan
B1-1
2
W-Mo deposit
Baizhangyan
B3-1
3
W-Mo deposit
Baizhangyan
B5-6-1
4
W-Mo deposit
Baizhangyan
B5-6-2
5
W-Mo deposit
Baizhangyan
B3-7
Sample/ REE chondrite
6
W-Mo deposit
Jitoushan
JTS27
7
W-Mo deposit
Jitoushan
P580-5
8
W-Mo deposit
Jitoushan
P510-4
REE pattern of scheelite
REE pattern of metallogenetic rocks
REE pattern of garnet

FIGURE. 6

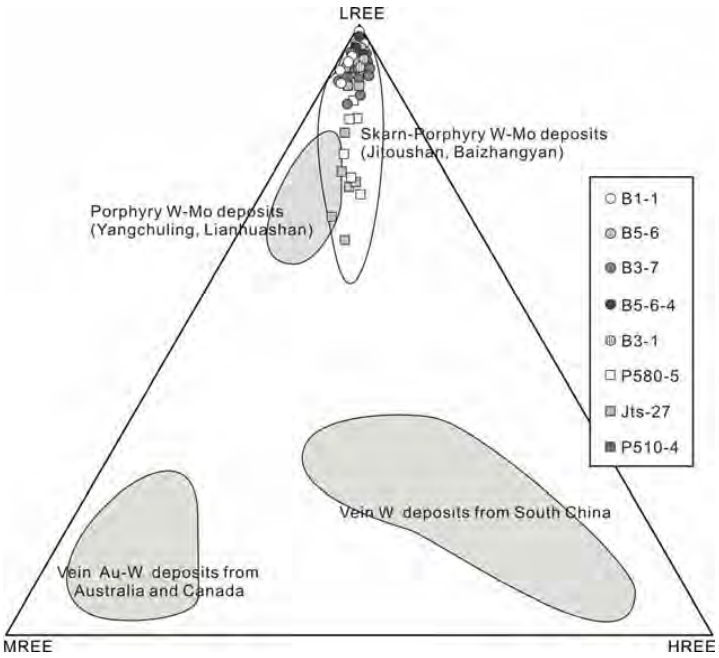
LREE
Skarn-Porphyry W-Mo deposits
(Jiroushan, Baizhangyan)
Porphyry W-Mo deposits
(Yangchuling, Lianhuashan)
B1-1
B5-6
B3-7
B5-6-4
B3-1
P580-5
Jts-27
P510-4
Vein W deposits from South China
Vein Au-W deposits from
Australia and Canada
MREE
HREE

FIGURE. 7

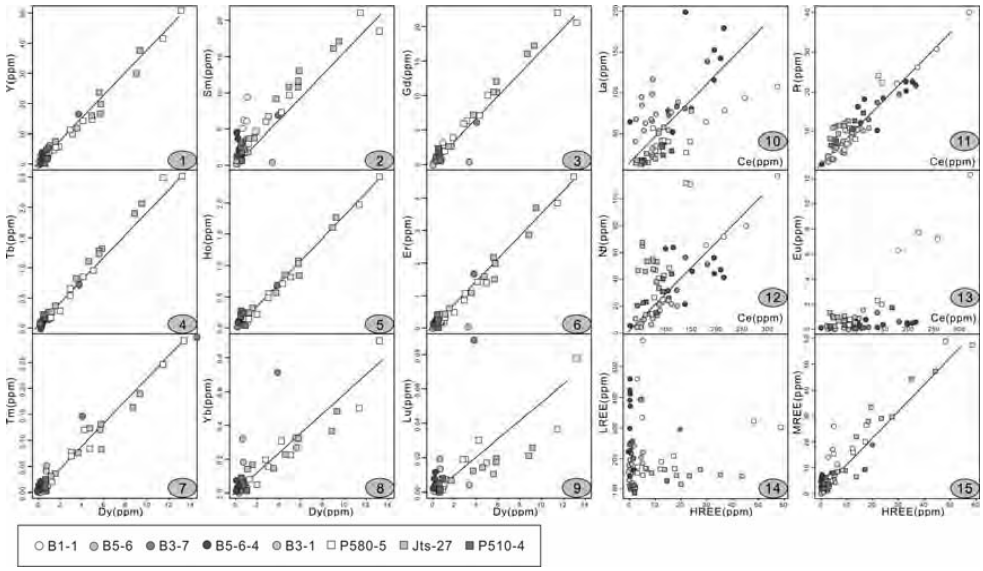
Y(ppm)
Sm(ppm)
Gd(ppm)
La(ppm)
Pr(ppm)
Tb(ppm)
Ho(ppm)
Er(ppm)
Nd(ppm)
Eu(ppm)
Tm(ppm)
Yb(ppm)
Lu(ppm)
LREE(ppm)
MREE(ppm)
Dy(ppm)
Ce(ppm)
HREE(ppm)
1
2
3
4
5
6
7
8
9
10
11
12
13
14
15
B1-1 B5-6 B3-7 B5-6-4 B3-1 P580-5 Jts-27 P510-4

FIGURE. 8

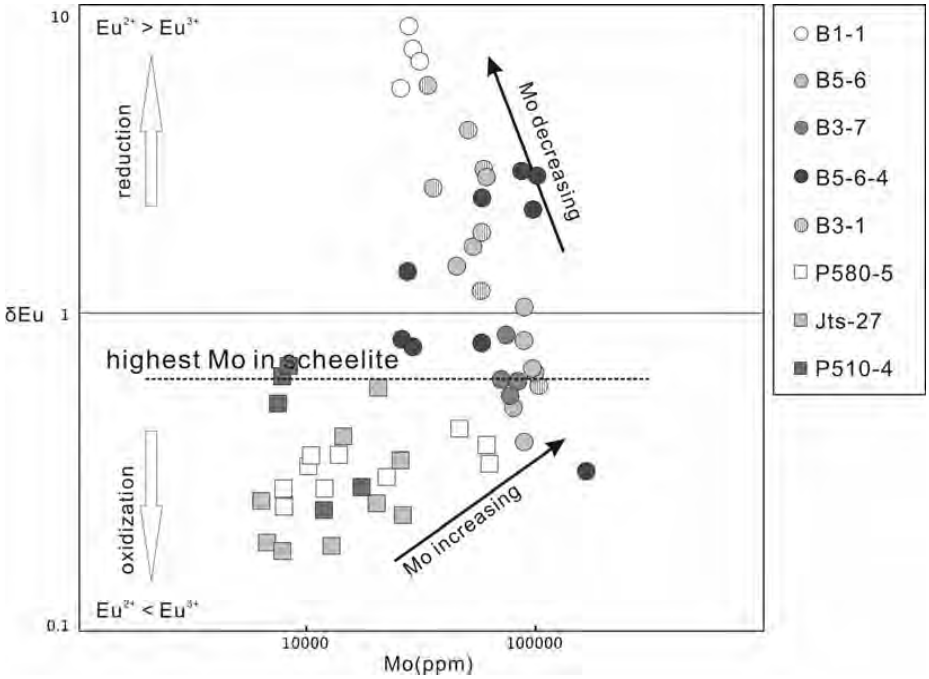
10
$Eu^{2+} > Eu^{3+}$
reduction
Mo decreasing
δEu 1
highest Mo in scheelite
oxidization
Mo increasing
$Eu^{2+} < Eu^{3+}$
0.1
10000
100000
Mo(ppm)
B1-1
B5-6
B3-7
B5-6-4
B3-1
P580-5
Jts-27
P510-4

FIGURE. 9

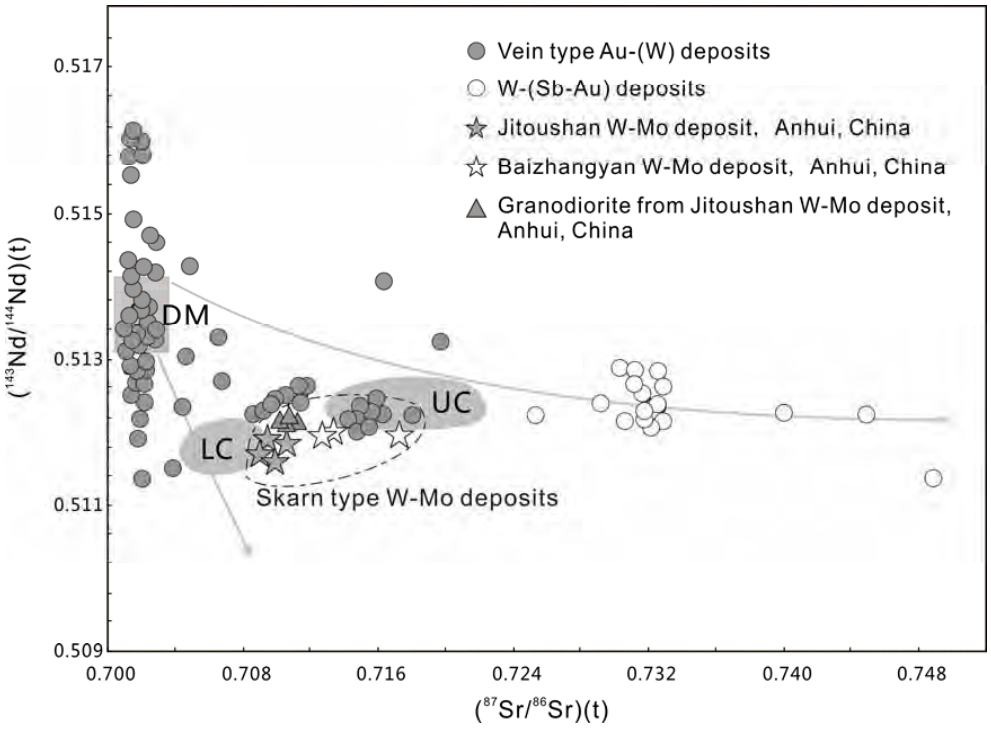
Vein type Au-(W) deposits
W-(Sb-Au) deposits
Jitoushan W-Mo deposit, Anhui, China
Baizhangyan W-Mo deposit, Anhui, China
Granodiorite from Jitoushan W-Mo deposit, Anhui, China
DM
UC
LC
Skarn type W-Mo deposits
0.517
0.515
0.513
0.511
0.509
0.700
0.708
0.716
0.724
0.732
0.740
0.748
(143Nd/144Nd)(t)
(87Sr/86Sr)(t)

FIGURE. 10

Table 1. Results of scheelite major element analysis from the Baizhangyan and Jitoushan W-Mo deposits in the Chizhou area, Eastern China (%).

No.	MoO_3	ZnO	PbO	WO_3	CaO	CuO	FeO	MnO	Total
Bzy-1	1.08	0	0	79.12	19.05	0	0.059	0.022	99.3
Bzy-2	2.02	0	0	78.24	19.73	0	0.032	0.012	100.0
Bzy-3	5.18	0.003	0.011	75.08	19.12	0	0.009	0.078	99.5
Bzy-4	2.87		0	77.71	19.55	0	0	0.011	100.1
Bzy-5	4.31	0.037	0	75.75	19.73	0	0.165	0.014	100.0
Jts-1	0.43	0.041	0	79.31	19.55	0.065	0.447	0.046	99.9
Jts-2	0.39	0.113	0.003	81.67	19.61	0.007	0.036	0.01	101.8
Jts-3	1.21	0.063	0.069	79.99	19.16	0	0.012	0	100.5
Jts-4	0.53	0.213	0.002	81.21	19.60	0.008	0	0.02	101.6
Jts-5	1.67	0.011	0	79.22	19.11	0	0.042	0	100.0
Jts-6	3.31	0.023	0.006	77.25	19.33	0	0	0.023	99.9
Jts-7	3.55	0.018	0.007	76.99	19.31	0	0	0.026	99.9
Jts-8	1.87	0.063	0.065	78.18	19.10	0	0.012	0	99.3
Jts-9	0.70	0.012	0.005	80.14	19.50	0.014	0.043	0.031	100.4

Note: Detection limit of EMP is 0.01%.

Table 2. Results of scheelite REE and trace element analysis from the Baizhangyan and Jitoushan W-Mo deposits in the Chizhou area, Eastern China (*ppm).

Sample NO.	La	Ce	Pr	Nd	Sm	Eu	Gd	Tb	Dy	Ho	Er	Tm	Yb	Lu	ΣREE+Y	δEu
B1-1-01	78.29	217.7	26.47	71.08	6.060	7.865	2.195	0.159	0.861	0.083	0.162	0.016	0.032	0.002	411.0	6.59
B1-1-02	106.4	321.4	40.12	116.9	9.578	12.23	2.957	0.243	0.936	0.096	0.189	0.020	0.064	< LOD	611.2	7.02
B1-1-03	92.19	257.4	30.80	79.81	5.096	7.140	1.260	0.108	0.471	0.043	0.109	0.007	0.030	0.002	474.5	8.61
B1-1-04	64.68	180.9	22.38	65.76	6.182	6.229	2.032	0.178	0.719	0.100	0.185	0.023	0.060	0.006	349.4	5.37
B5-6-01	97.80	73.25	4.890	7.17	0.370	0.110	0.776	0.049	0.231	0.051	0.073	0.001	0.016	< LOD	184.8	0.63
B5-6-02	61.98	61.90	5.988	13.36	0.675	0.167	0.540	0.021	0.104	0.032	0.021	0.007	0.007	< LOD	144.8	0.85
B5-6-03	65.88	75.49	7.630	14.28	0.303	0.263	0.273	0.007	3.358	< LOD	0.004	< LOD	0.000	0.004	167.5	2.79
B5-6-04	66.73	73.27	7.303	14.03	0.280	0.132	0.205	0.001	0.009	0.004	< LOD	< LOD	0.030	< LOD	162.0	1.68
B5-6-05	115.4	76.21	4.951	11.60	1.765	0.431	1.856	0.231	0.997	0.140	0.260	0.024	0.044	0.006	213.9	0.73
B5-6-06	84.26	54.76	3.266	3.81	0.260	0.095	0.273	0.025	0.101	0.016	0.012	0.005	0.038	< LOD	146.9	1.09
B5-6-07	54.93	58.83	5.419	9.82	0.191	0.117	0.084	0.004	0.020	0.002	0.007	< LOD	< LOD	< LOD	129.4	2.81
B5-6-08	94.23	52.19	3.146	6.54	1.251	0.175	1.419	0.133	0.494	0.074	0.144	0.009	< LOD	< LOD	159.8	0.40
B5-6-09	73.41	82.44	7.270	13.63	0.306	0.132	0.250	0.006	0.030	0.001	0.004	0.001	< LOD	< LOD	177.5	1.46
B5-6-10	68.89	43.12	2.666	4.07	0.540	0.099	0.575	0.042	0.283	0.031	0.064	0.007	0.019	0.002	120.4	0.54
B3-7-1-01	72.75	107.9	11.78	26.43	1.095	0.219	0.511	0.012	0.089	< LOD	0.000	0.000	0.018	< LOD	220.8	0.90
B3-7-1-02	83.19	123.4	13.12	32.03	1.208	0.179	0.648	0.019	0.139	0.009	0.028	0.004	0.013	< LOD	254.0	0.62
B3-7-1-03	80.80	140.5	17.41	56.43	6.911	1.328	6.084	0.719	3.793	0.691	1.662	0.147	0.712	0.088	317.3	0.63
B3-7-1-04	139.6	183.5	19.50	51.32	3.633	0.594	2.602	0.175	0.703	0.103	0.179	0.014	0.064	0.003	402.0	0.59
B5-6-4-01	152.6	197.3	20.32	44.36	0.859	0.495	0.542	0.021	0.035	< LOD	0.053	0.006	0.071	0.003	416.7	2.22
B5-6-4-02	40.08	102.3	16.33	63.43	3.564	0.611	1.295	0.055	0.171	0.010	< LOD	< LOD	0.020	< LOD	227.8	0.87
B5-6-4-03	198.9	140.7	10.29	21.29	1.847	0.144	1.099	0.058	0.209	0.016	0.020	0.003	< LOD	< LOD	374.6	0.31
B5-6-4-04	52.04	115.2	18.24	64.46	4.392	0.661	1.321	0.082	0.045	0.045	0.003	< LOD	< LOD	0.004	256.5	0.84

B5-6-2-01	142.4	209.8	22.61	47.27	0.671	0.496	0.388	0.023	0.014	0.007	0.011	< LOD	< LOD	< LOD	423.7	2.97
B5-6-2-02	115.5	196.7	22.63	56.18	1.548	0.397	0.161	0.022	0.071	0.007	0.032	0.003	< LOD	0.007	393.2	2.43
B5-6-2-03	179.1	216.3	21.75	41.45	1.254	0.581	0.299	0.037	0.077	0.016	< LOD	0.013	< LOD	0.013	460.9	2.90
B5-6-2-04	80.79	152.0	18.44	46.71	1.208	0.357	0.524	0.001	0.101	< LOD	0.017	0.001	< LOD	< LOD	300.2	1.37
B5-6-5-01	78.20	106.3	12.02	31.88	1.385	0.288	0.801	0.063	0.047	0.012	0.021	< LOD	< LOD	< LOD	231.0	0.84
B5-6-7-01	64.34	31.55	1.874	5.605	0.787	0.163	0.474	0.024	0.135	0.029	0.024	0.005	0.029	0.002	105.0	0.81
B3-1-1-01	51.44	90.53	9.484	22.16	1.289	0.621	0.420	0.054	0.126	0.031	0.098	0.009	0.029	0.002	176.3	2.58
B3-1-1-02	54.08	106.8	10.88	24.54	0.789	0.812	0.258	0.016	0.076	0.010	0.008	0.002	0.030	< LOD	198.3	5.50
B3-1-1-03	40.75	42.22	3.633	10.82	1.186	0.169	0.631	0.046	0.200	0.026	0.069	0.000	0.006	< LOD	99.75	0.60
B3-1-3-01	56.59	95.70	9.728	23.29	1.446	0.965	0.990	0.107	0.626	0.101	0.324	0.049	0.320	0.019	190.3	2.47
B3-1-3-02	87.05	124.2	10.90	20.18	0.772	0.272	0.586	0.057	0.256	0.037	0.112	0.017	0.076	0.003	244.5	1.24
B3-1-3-03	76.29	112.6	10.22	21.89	1.676	1.543	0.886	0.149	0.697	0.100	0.250	0.041	0.182	0.014	226.6	3.87
B3-1-3-04	52.33	90.10	8.674	17.08	0.843	0.360	0.441	0.037	0.127	0.027	0.090	0.012	0.054	0.002	170.2	1.81
P580-5-1-01	28.26	87.95	10.64	41.21	4.744	0.535	4.005	0.295	1.862	0.230	0.505	0.000	0.051	< LOD	180.3	0.38
P580-5-1-02	35.38	79.50	7.211	25.91	2.990	0.330	2.696	0.284	1.103	0.156	0.389	0.021	0.079	< LOD	156.1	0.36
P580-5-1-03	41.18	106.9	11.80	49.08	7.132	0.794	7.214	0.856	4.207	0.717	1.434	0.123	0.311	0.029	231.8	0.34
P580-5-3-01	41.53	98.41	10.53	42.09	6.106	0.572	6.007	0.548	2.894	0.498	0.880	0.068	0.196	0.018	210.3	0.29
P580-5-3-02	27.63	79.72	10.45	47.44	6.836	0.667	6.424	0.664	3.005	0.564	1.035	0.075	0.160	0.020	184.7	0.31
P580-5-2-01	56.97	76.57	5.152	13.88	1.270	0.145	0.925	0.116	0.423	0.104	0.170	0.017	0.065	< LOD	155.8	0.41
P580-5-2-02	24.20	76.80	10.72	54.08	9.766	0.811	10.15	0.964	4.933	0.822	1.413	0.088	0.229	0.016	195.0	0.25
P580-5-2-03	42.68	95.76	8.338	24.79	2.401	0.331	2.160	0.187	0.848	0.144	0.245	0.017	0.062	0.002	178.0	0.44
P580-5-5-01	26.83	141.1	24.25	112.1	18.58	2.339	20.66	2.518	13.09	2.430	4.677	0.293	0.904	0.078	369.9	0.36
P580-5-5-02	41.18	149.5	22.52	111.2	21.14	2.044	22.11	2.454	11.35	1.986	3.869	0.249	0.493	0.037	390.2	0.29
JTS-27-2-01	13.59	47.3	8.336	46.59	13.00	1.244	12.08	1.289	5.665	0.838	1.499	0.081	0.322	0.019	151.9	0.30
JTS-27-2-02	12.91	52.99	11.09	66.20	17.12	1.034	17.26	2.061	9.311	1.768	3.696	0.190	0.482	0.025	196.1	0.18
JTS-27-2-03	12.68	54.69	11.12	66.41	16.12	0.937	16.34	1.898	8.824	1.619	2.869	0.160	0.366	0.020	194.1	0.18

JTS-27-2-04	35.50	90.08	10.43	32.50	3.736	0.657	2.655	0.277	1.063	0.218	0.380	0.032	0.150	0.007	177.7	0.64
JTS-27-2-05	30.04	75.70	11.03	47.77	9.183	1.080	7.194	0.821	3.555	0.565	1.092	0.075	0.150	0.012	188.3	0.41
JTS-27-1-01	16.91	57.24	7.757	23.67	2.304	0.215	1.619	0.142	0.542	0.082	0.148	0.006	0.014	0.001	110.7	0.34
JTS-27-1-02	24.61	64.01	9.476	47.09	11.06	0.919	10.03	1.107	4.715	0.849	1.582	0.120	0.229	0.014	175.8	0.27
JTS-27-4-01	19.35	83.36	12.39	38.08	3.791	0.276	2.887	0.368	1.538	0.323	0.614	0.036	0.166	0.007	163.2	0.25
JTS-27-4-02	21.34	76.34	12.15	54.39	11.40	0.855	10.53	1.261	5.569	1.074	2.187	0.122	0.270	0.011	197.5	0.24
JTS-27-4-03	14.79	64.52	11.55	53.45	10.79	0.655	10.51	1.308	5.729	1.033	2.039	0.132	0.312	0.018	176.8	0.19
P510-4-3-01	17.04	58.29	7.186	22.54	1.220	0.163	0.393	0.016	0.088	< LOD	0.012	< LOD	< LOD	< LOD	106.9	0.72
P510-4-3-02	13.52	49.52	6.630	20.54	1.450	0.193	0.813	0.080	0.297	0.054	0.025	0.016	0.065	0.006	93.20	0.54
P510-4-3-03	15.66	58.86	7.781	23.30	1.089	0.137	0.262	0.018	0.044	0.007	0.021	0.001	0.008	< LOD	107.2	0.78
P510-4-2-01	24.05	96.21	12.75	40.44	2.921	0.165	1.525	0.133	0.358	0.056	0.058	0.004	< LOD	< LOD	178.7	0.24
P510-4-2-02	29.01	113.3	14.74	44.14	3.030	0.202	1.621	0.129	0.474	0.053	0.093	0.000	< LOD	0.005	206.8	0.28
P510-4-2-03	33.03	95.93	10.75	29.70	2.130	0.137	0.967	0.079	0.286	0.053	0.061	0.003	< LOD	< LOD	173.1	0.29

Table 2 (continued)

Sample NO.	Mo	Sn	Ba	Cu	Zn	Pb	Bi	Rb	Sr	Y	LREE/HREE	LREE	MREE	HREE
B1-1-01	31044	0.081	0.393	< LOD	< LOD	5.26	0.033	0.091	41	4.199	116.2	393.55	17.139	0.293
B1-1-02	30514	0.087	0.280	< LOD	< LOD	5.60	0.112	0.017	41	4.798	134.6	584.86	25.941	0.371
B1-1-03	27995	0.123	0.342	< LOD	4.19	4.40	0.046	< LOD	40	2.685	232.7	460.20	14.074	0.192
B1-1-04	25909	0.051	0.294	1.66	1.57	3.99	0.021	< LOD	35	4.545	104.8	333.70	15.339	0.373
B5-6-01	100832	0.007	0.844	0.00	< LOD	4.40	0.044	0.081	93	0.744	153.2	183.11	1.536	0.142
B5-6-02	89828	< LOD	0.742	2.03	< LOD	4.21	0.058	0.057	136	0.386	197.0	143.23	1.507	0.066
B5-6-03	60611	0.192	0.773	0.00	< LOD	3.83	< LOD	0.129	84	< LOD	44.94	163.28	4.204	0.008

B5-6-04	54299	0.083	0.166	8.05	29.24	3.66	0.053	< LOD	84	< LOD	648.8	161.34	0.627	0.035
B5-6-05	97873	0.060	1.182	4.66	15.88	3.86	0.118	0.074	89	4.076	59.10	208.12	5.279	0.475
B5-6-06	89996	0.014	0.868	10.93	1.46	4.94	0.030	0.085	84	0.588	310.5	146.10	0.755	0.072
B5-6-07	59361	0.178	0.512	10.84	0.00	3.17	0.030	0.157	78	< LOD	1108	129.00	0.415	0.009
B5-6-08	89851	< LOD	0.766	< LOD	11.50	35.29	1.855	0.120	86	2.052	69.33	156.10	3.472	0.227
B5-6-09	46021	0.070	0.475	3.96	0.00	3.58	0.006	0.073	76	0.036	607.1	176.74	0.724	0.006
B5-6-10	80532	0.264	0.621	0.00	13.12	3.31	0.010	0.105	80	1.130	116.8	118.75	1.539	0.123
B3-7-1-01	74213	< LOD	0.678	16.80	17.40	3.08	0.019	0.244	131	0.542	349.0	218.83	1.927	0.018
B3-7-1-02	79966	0.116	1.031	< LOD	18.60	6.50	3.584	0.131	147	0.438	294.3	251.76	2.194	0.054
B3-7-1-03	72269	0.183	0.832	< LOD	< LOD	4.84	0.826	0.082	155	16.53	21.83	295.16	18.835	3.300
B3-7-1-04	79877	0.166	1.083	< LOD	13.09	109.00	83.324	< LOD	102	3.831	103.6	393.91	7.706	0.363
B5-6-4-01	96996	0.262	1.271	< LOD	< LOD	7.91	0.067	0.047	140	0.137	569.4	414.57	1.952	0.132
B5-6-4-02	26183	0.114	0.246	< LOD	< LOD	3.85	0.021	< LOD	234	0.015	145.9	222.10	5.696	0.030
B5-6-4-03	177815	0.618	1.809	< LOD	1.59	8.52	0.027	< LOD	162	0.303	265.7	371.24	3.357	0.039
B5-6-4-04	27881	0.367	0.528	< LOD	< LOD	4.27	< LOD	< LOD	244	0.446	170.1	249.99	6.501	0.051
B5-6-2-01	84749	0.195	0.809	< LOD	7.39	8.67	0.048	< LOD	152	0.176	955.1	422.06	1.592	0.018
B5-6-2-02	58231	0.093	0.764	< LOD	6.42	7.32	0.030	< LOD	157	0.189	1292	390.99	2.200	0.050
B5-6-2-03	98434	0.430	0.578	< LOD	3.25	8.65	0.143	0.161	128	0.220	1014	458.65	2.248	0.041
B5-6-2-04	28806	< LOD	0.367	0.33	18.61	5.08	0.036	0.244	142	0.160	465.4	297.99	2.191	0.018
B5-6-5-01	57895	0.206	0.541	< LOD	< LOD	4.45	0.000	< LOD	132	0.298	243.6	228.38	2.584	0.033

B5-6-7-01	96853	< LOD	1.224	< LOD	< LOD	5.05	0.089	0.031	98	0.393	144.5	103.36	1.583	0.089
B3-1-1-01	35796	0.175	0.817	1.79	1.46	5.06	0.379	< LOD	72	0.781	228.2	173.62	2.511	0.169
B3-1-1-02	33412	< LOD	0.534	< LOD	0.00	4.45	0.115	0.058	64	0.187	492.2	196.27	1.952	0.052
B3-1-1-03	100945	0.146	1.452	< LOD	10.35	2.62	0.067	< LOD	178	0.786	101.0	97.42	2.232	0.101
B3-1-3-01	54550	0.221	0.499	2.09	< LOD	3.82	0.372	0.132	132	4.316	73.97	185.31	4.135	0.814
B3-1-3-02	57175	0.159	0.784	< LOD	< LOD	3.31	1.173	0.088	177	1.525	212.9	242.30	1.942	0.245
B3-1-3-03	51266	0.150	0.523	< LOD	< LOD	3.67	0.144	0.110	119	4.674	96.74	221.02	4.950	0.587
B3-1-3-04	58035	0.101	0.506	8.42	8.75	2.91	0.255	< LOD	146	0.974	214.3	168.19	1.808	0.185
P580-5-1-01	13147	0.229	< LOD	2.64	< LOD	1.99	< LOD	< LOD	280	5.970	24.95	168.07	11.440	0.787
P580-5-1-02	59546	0.209	0.435	6.29	5.86	1.73	< LOD	0.428	184	4.093	32.01	148.01	7.403	0.644
P580-5-1-03	10094	0.051	0.238	0.00	11.02	1.52	< LOD	< LOD	227	14.46	14.57	208.98	20.203	2.615
P580-5-3-01	8420	0.276	0.102	6.40	13.34	1.77	0.010	0.087	170	10.74	17.93	192.55	16.127	1.661
P580-5-3-02	22575	0.173	0.234	< LOD	18.63	1.67	0.013	< LOD	183	10.33	14.46	165.24	17.597	1.853
P580-5-2-01	58208	0.077	0.469	< LOD	14.83	2.13	0.028	0.083	153	2.400	84.59	152.58	2.878	0.357
P580-5-2-02	8042	0.141	0.134	11.29	2.97	1.64	< LOD	0.105	192	14.94	9.478	165.80	26.619	2.568
P580-5-2-03	47099	0.220	0.315	2.90	8.12	1.82	0.058	< LOD	214	2.924	47.57	171.57	5.926	0.470
P580-5-5-01	10408	< LOD	0.152	11.58	0.80	1.94	< LOD	0.165	123	50.29	7.284	304.32	57.191	8.383
P580-5-5-02	12262	0.024	0.190	2.90	9.19	5.23	0.801	< LOD	122	41.53	8.170	324.45	59.096	6.633
JTS-27-2-01	9092	0.263	0.228	1.13	< LOD	2.40	0.010	0.316	377	17.26	5.971	115.86	33.272	2.758
JTS-27-2-02	6779	0.195	0.269	22.81	< LOD	5.39	0.097	0.037	277	37.58	4.637	143.19	46.794	6.162

JTS-27-2-03	7390	0.139	0.164	6.63	< LOD	1.99	0.010	< LOD	298	29.91	5.047	144.90	44.119	5.034
JTS-27-2-04	20356	0.060	0.695	< LOD	14.07	2.22	0.022	0.153	493	5.554	36.15	168.50	8.388	0.787
JTS-27-2-05	13663	0.121	0.633	< LOD	7.60	2.94	0.012	0.110	468	11.72	12.98	164.53	21.833	1.894
JTS-27-1-01	25597	0.231	0.645	5.02	< LOD	2.23	0.019	0.344	414	1.467	42.33	105.58	4.822	0.252
JTS-27-1-02	6777	0.095	0.277	6.01	4.04	2.44	< LOD	0.318	292	15.46	8.431	145.19	27.829	2.794
JTS-27-4-01	19953	0.042	0.545	13.33	0.00	2.24	0.012	< LOD	422	7.506	26.48	153.18	8.859	1.145
JTS-27-4-02	26008	0.086	0.438	< LOD	21.49	1.81	< LOD	0.153	355	23.74	8.393	164.22	29.622	3.664
JTS-27-4-03	12835	0.067	0.164	8.24	< LOD	1.30	< LOD	< LOD	298	19.74	7.389	144.30	28.986	3.534
P510-4-3-01	7484	0.413	0.389	3.86	< LOD	2.00	< LOD	0.115	373	0.338	209.0	105.06	1.879	0.013
P510-4-3-02	6784	1.336	0.426	5.62	1.63	1.61	0.015	0.351	349	1.329	67.69	90.21	2.833	0.167
P510-4-3-03	6698	0.063	0.308	0.00	4.80	2.17	< LOD	0.016	364	0.110	294.9	105.60	1.551	0.038
P510-4-2-01	10830	0.229	0.429	5.24	< LOD	2.15	< LOD	0.185	425	0.978	82.69	173.45	5.103	0.118
P510-4-2-02	11341	0.085	0.218	< LOD	2.89	2.19	< LOD	< LOD	436	1.005	86.05	201.16	5.457	0.151
P510-4-2-03	15978	< LOD	0.521	22.57	9.28	2.30	0.049	< LOD	407	0.911	118.6	169.40	3.599	0.116

Note: LOD Limit of detection calculated from repeated measurements of NIST610: La, Ce, Pr, Nd, Sm, Eu, Gd, Tb, Dy, Ho, Er, Tm, Yb and Lu= 0.001 ppm; Y, Nb, Sm, Pb, Ba, Cu, Zn, Bi, Sn,and Rb =0.01 ppm; Sr = 0.02 ppm; and Mo = 0.03 ppm.

Table 3. Results of scheelite Sr-Nd isotopic analysis from the Baizhangyan and Jitoushan W-Mo deposits in the Chizhou area, Eastern China.

Sample No.	weight (g)	Sm(ppm)	Nd(ppm)	Sr(ppm)	$^{147}Sm/^{144}Nd$	$^{143}Nd/^{144}Nd$	2sigma	$(^{143}Nd/^{144}Nd)(t)$	εNd(t)	$(^{87}Sr/^{86}Sr)(t)$	2sigma
Jitoushan								T=137Ma (Song et al., 2012a)			
p580-5	0.0273	1.901	15.42	349.2	0.07455	0.51190	0.000008	0.51183	-12.3	0.70956	0.0009
P510-4	0.0363	2.012	9.24	298.6	0.13169	0.51176	0.000010	0.51164	-16.0	0.70974	0.0012
JT49	0.0243	1.131	10.19	533.1	0.06712	0.51181	0.000012	0.51175	-13.9	0.70949	0.0008
JTS-27	0.0364	0.837	9.54	186.8	0.05302	0.51178	0.000012	0.51173	-14.2	0.70946	0.0007
Baizhangyan								T=134Ma (Song et al., 2012b)			
B3-1	0.0226	1.750	19.10	89.79	0.05539	0.51203	0.000015	0.51198	-9.5	0.71245	0.0010
B5-2	0.0463	1.958	26.23	212.3	0.04513	0.51204	0.000009	0.51200	-9.1	0.71367	0.0007
B5-6-2	0.0147	2.851	20.72	179.2	0.08318	0.51206	0.000014	0.51199	-9.3	0.71738	0.0010

Table 4. Comparison of scheelite Sr-Nd isotopic analyses from hydrothermal deposits around the world.

Deposit	Area	Ore types	Samples NO.	$^{143}Nd/^{144}Nd(t)$	$^{87}Sr/^{86}Sr(t)$	From
Felbertal tungsten deposit	Austria,Central Alps	vein type	HEJ 27	0.51236	0.72962	Eichhorn et al.,1997
			HEJ 25	0.51226	0.72553	
			TS 1024	0.51227	0.75530	
			ZONE 1110	0.51225	0.74514	
			19845	0.51257	0.79432	
			1110 K1	0.51227	0.74023	
			1175 K2	0.51234	0.79204	
Bjorkdal Au deposit	Northern Sweden	vein type	2-91	0.51349	0.70260	Billstrom et al., 2009
			2-91B	0.51331	0.70250	
			108	0.51467	0.70250	
			103b1	0.51336	0.70270	
			308-92	0.51332	0.70260	
			EJ-1	0.51370	0.70260	
			306	0.51462	0.70250	
Au-W deposits	Zimbabwe	vein type				Darbyshire et al., 1996
			Dainy-1	0.51303	0.70460	
			Joe's Luck	0.51363	0.70180	
			GBH	0.51415	0.70226	
			Symington	0.51303	0.70456	
			Hahnie	0.51435	0.70480	
			White Heather	0.51289	0.70147	
			Golden Valley	0.51247	0.70469	
			Patchway	0.51324	0.70151	

			Homestead Tungsten	0.51336	0.70652	
			Scheelite King	0.51143	0.70469	
			White Stork	0.51132	0.70206	
			Aaffaire	0.51190	0.70184	
			Badger and Pheasant	0.51242	0.70175	
			Tea Tea	0.51218	0.70778	
			Central C	0.51267	0.70689	
			Brompton	0.51215	0.71803	
			Brompton-1	0.51323	0.71965	
			Scheelite Prince claims	0.51406	0.71630	
			Old Grand Parade	0.51276	0.70649	
			Phoenix	0.51885	0.71252	
Omai gold deposit	Guiana	vein type	Sch-Q01	0.51223	0.70202	Voicu et al., 2000
			Sch-Q08	0.51286	0.70203	
			350Sch	0.51382	0.70204	
			376Sch	0.51303	0.70198	
			Sch-Q07	0.51252	0.70210	
			Sch	0.51245	0.70196	
			Sch-Q05	0.51344	0.70201	
Archaean gold deposits	Western Australia	vein type	MC7-1	0.51341	0.70130	Brugger et al., 2002
			MC7-2	0.51420	0.70163	
			MC7-3	0.51395	0.70153	
			97MC8-1	0.51610	0.70144	
			97MC8-2	0.51625	0.70141	
			97MC8-3	0.51580	0.70144	

			97MC8-4	0.51558	0.70146	
Archcan gold deposits	Canada	vein type	Lake Head	0.51279	0.70184	Bell et al., 1989
			Little Long Lac	0.51275	0.70174	
			Coniaurum-1	0.51275	0.70166	
			Coniaurum-2	0.51281	0.70167	
			Hollinger-1	0.51328	0.70159	
			Hollinger-2	0.51342	0.70165	
			Hollinger-3	0.51361	0.70183	
			Hollinger-4	0.51280	0.70165	
			Mcintyre	0.51516	0.70227	
Muruntau Au-W deposit	Uzbekistan	vein type	MT3773	0.51227	0.71503	Kempe et al., 2001
			MT3776	0.51208	0.71465	
			MT3778	0.51205	0.71497	
			MT3779	0.51217	0.71456	
			MT1	0.51219	0.71538	
			MT1A	0.51220	0.71525	
			MT2	0.51221	0.71491	
			MT3423	0.51214	0.71559	
			MT76-276	0.51209	0.71562	
			MT876	0.51206	0.71510	
			MT7	0.51209	0.71473	
			MT80-532	0.51222	0.71623	
Mount Charlotte deposit	Australia	vein type	91-232	0.51431	0.70140	Kent et al., 1995
			93-1195	0.51591	0.70144	
			93-1196	0.51598	0.70134	
			93-1197	0.51333	0.70145	

			93-1199	0.51413	0.70145	
Woxi W-Sb-Au deposit	Hunan, China	vein type	V4M	0.51133	0.74836	Peng et al.,2006
Zhazi W-Sb deposit	Hunan, China	vein type	ZX-35	0.51288	0.73036	Peng et al.,2008
			ZX-36	0.51285	0.73155	
			ZX-15	0.51225	0.73199	
			ZX-16	0.51221	0.73266	
			ZX-20	0.51217	0.73276	
			ZX-7	0.51220	0.73192	
			ZX-8	0.51217	0.73267	
			ZX-28	0.51224	0.73225	
			ZX-29	0.51285	0.73274	
			ZX-30	0.51271	0.73295	
			ZX-31	0.51253	0.73186	
			ZX-22	0.51211	0.73242	
			ZX-23	0.51211	0.73216	
			ZX-24	0.51234	0.73245	
			ZX-1	0.51216	0.73043	
Daping Au deposit	Yunan,China	vein type	4101	0.51224	0.70940	Xiong et al., 2006
			4107	0.51221	0.70880	
			4113	0.51221	0.70940	
			4114	0.51223	0.70970	
			4129	0.51232	0.71120	
			4130	0.51229	0.71080	